



REEL Demo – Romande Energie ELectric network in local balance Demonstrator

Deliverable: 5d2 Detailed evaluation of the grid operation
bottlenecks and load shifting potential for the reference
system

Demo site: Rolle

Developed by

Luise MIDDELHAUVE (EPFL-IPESE)

Lionel BLOCH (EPFL-PVlab)

Jordan HOLWEGER (EPFL-PVlab)

Paul STADLER (EPFL-IPESE)

Luc GIRARDIN (EPFL-IPESE)

In collaboration with

Hochschule Luzern (HSLU)

Romande Energie (RE)

[Sion/Neuchâtel, 27.04.2019]

Contents

- 1 Executive summary** **4**

- 2 Description of deliverable and goal** **5**
 - 2.1 Introduction 5
 - 2.2 Research question 7
 - 2.3 Novelty of the proposed solutions compared to the state-of-art 8
 - 2.4 Description of the deliverable 8

- 3 Achievement of Deliverable** **9**
 - 3.1 Date 9
 - 3.2 Demonstration of the Deliverable 9
 - 3.3 Impact 11

- 4 Research methodology** **12**
 - 4.1 Optimisation of the PV potential 12
 - Solar Roof post-processing 12
 - Roofs clustering 13
 - 4.2 Load profiles allocation model 16
 - First stage optimization 16
 - Second stage optimization 19
 - 4.3 Building multi-energy optimisation 21
 - Temporal data reduction 21
 - Main constraints of the MILP multi- objective building model 22
 - 4.4 Load shifting 26
 - Behavioural flexibility 26
 - Operational flexibility 33
 - Technical flexibility 35
 - 4.5 Grid stability assessment 35

- 5 Results** **37**
 - 5.1 Load allocation 37
 - 5.2 Building’s optimization results 38
 - 5.3 Load shifting potential 39
 - Behavioural flexibility 39
 - Theoretical behavioural flexibility equivalent storage 46

| | |
|---|-----------|
| Operational flexibility | 49 |
| Technical flexibility | 50 |
| 5.4 Grid operation bottlenecks | 51 |
| PV hosting capacity | 52 |
| Grid stability assessment under the deployment of a selected scenario | 53 |
| 6 Conclusion | 56 |

Nomenclature

ACRONYMS

| | |
|-----------|---|
| BES | Building energy system |
| CAPEX | Capital Expenditure |
| DSO | Distribution System Operators |
| G2P | Gas to power |
| GIS | Geographic Information System |
| GM | Grid Multiple |
| IRENA | International Renewable Energy Agency |
| LPEM | Low temperature Proton Exchange Membrane fuel cells |
| LV | Low Voltage |
| MILP | Mixed integer linear programming |
| MPC | Model Predictive Control |
| MV | Medium Voltage |
| OPEX | Operational Expense |
| P2G | Power to gas |
| PV | Photovoltaic |
| REel Demo | Romande Energie ELeetric network Demonstrator |
| SC | Self-consumption |
| SOFC | Solid Oxide Fuel Cells |
| SS | Self-suciency |

1. Executive summary

Based on the analysis of the reference case, models developed at the PVLAB-EPFL and IPESE-EPFL have been valued and improved to assess the impact of distributed generation and ancillary services on REel demonstrator. The models are used to evaluate solutions capable to cope with the variability and uncertainty of renewable energy generation, avoiding curtailment and reliably supplying all the demanded energy to customers.

The database compiled by the JA-RED partners [9], have been enhanced and converted into an essential tool to support communication and strategic decisions among the REel Demonstrator Community. This database contains for each building the typology, the actual energy agents, an estimation of the energy demand, the relation with the injection point of the energy distribution networks and the actual usage and potential of renewable energy such as the solar PV potential.

In order to evaluate the energy flow in the grid with sufficient precision, skills have been developed in the allocation of stochastic load profiles from aggregated measurements. Moreover, the profiles for PV generation have been refined considering the optimal roof's area and orientation. Methods to assess the power grid flexibility are based on both consumers behaviour and technical and operational flexibility. The assessment of the latest relies on a model recently developed for the generation optimal design and operation of energy technologies in buildings [16].

Finally, the limits imposed by the existing power supply infrastructure have been identified using a power flow algorithm to conduct grid stability assessment and detect the bottlenecks in the power grid. For this task, the stochastic nature of the proposed load profile allocation model is fundamental.

2. Description of deliverable and goal

2.1. Introduction

According to the International Energy Agency (IRENA), the share of renewable energy in the power sector could more than triple compared to current levels with a potential coverage by variable sources such as solar and wind energy reaching 60% of the total electricity production (Figure 1). This energy transition will indeed require large-scale electrification of end-use sectors (buildings, industry and transport) and a gradual decarbonisation of the power sector.

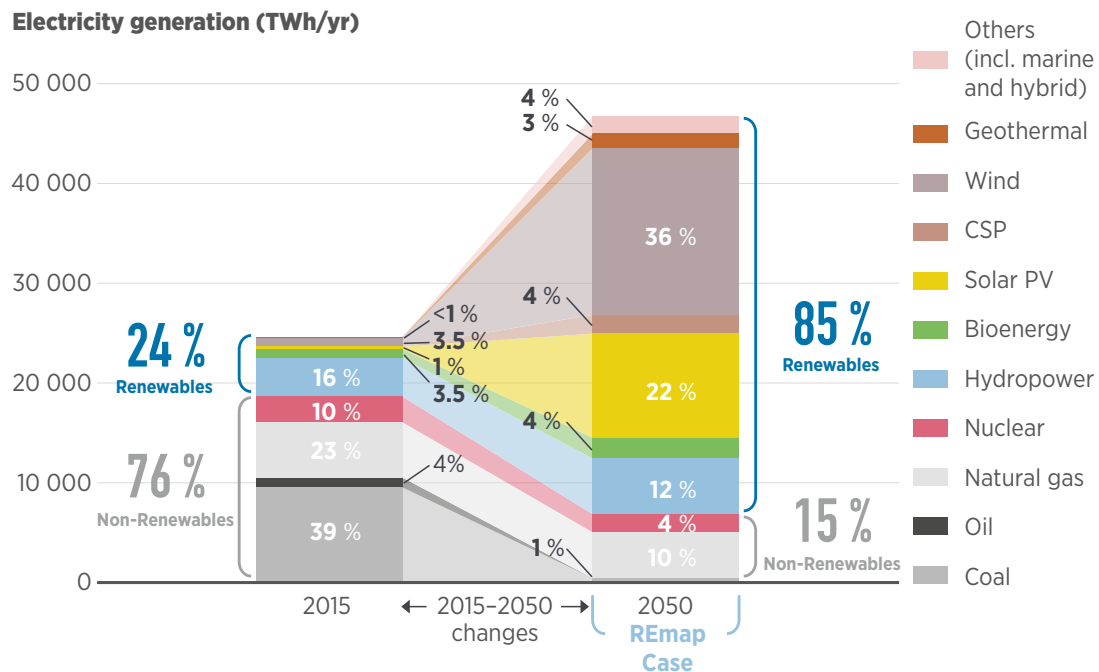


Figure 1: Worldwide electricity generation 2015–2050 (source: IRENA [4]).

At the Swiss level, the implementation of the EnergyStrategy 2050 [2] foresees a decrease in electricity consumption of 3% in 2020 and 13% in 2050 compared to 2020 with an amount of renewable production excluding hydropower of 4400 GWh in 2020 and 11'400 GWh in 2050 with in addition a stable hydropower production (37'400 GWh in 2050).

Assuming a constant development of the renewable energy mix (excluding hydropower) with a global growth rate of 67% between 2020 and 2050 [10] and an evolution of the Swiss population according to the reference scenario from [5], the share of renewable energy should reach 80% in 2050 with a contribution of 10% from photovoltaic (2).

However, according to Swissolar [17], the existing PV potential on roof and facades is much higher, ranging from 30'000 up to more than 50'000 GWh corresponding to 70% of the actual electricity demand.

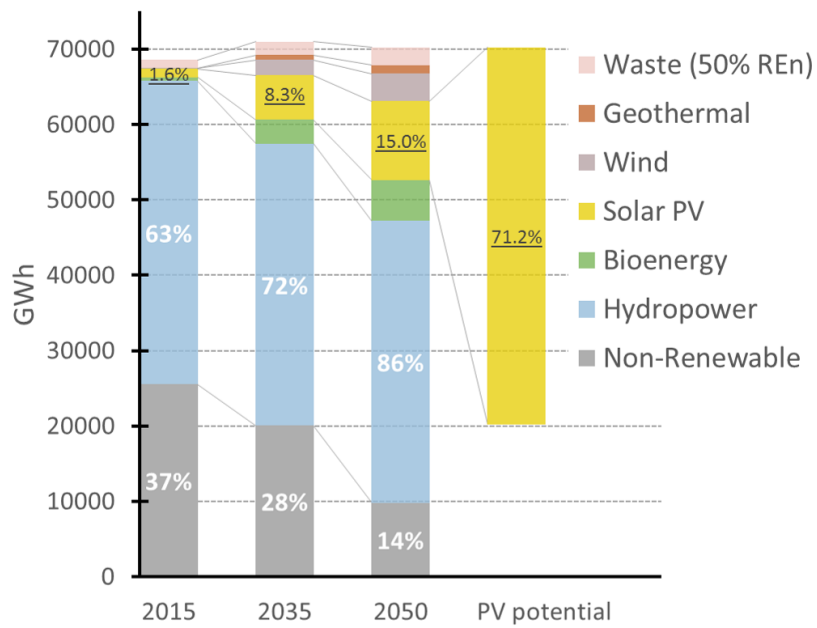


Figure 2: Swiss electricity generation strategy up to 2050 [2].

About 300 MW of PV per year have been installed during the period from 2012 to 2017. At this rate, 11.8 GW would be installed in 2050 generating 10.4 TWh per year covering about 15% of the Swiss annual electricity consumption.

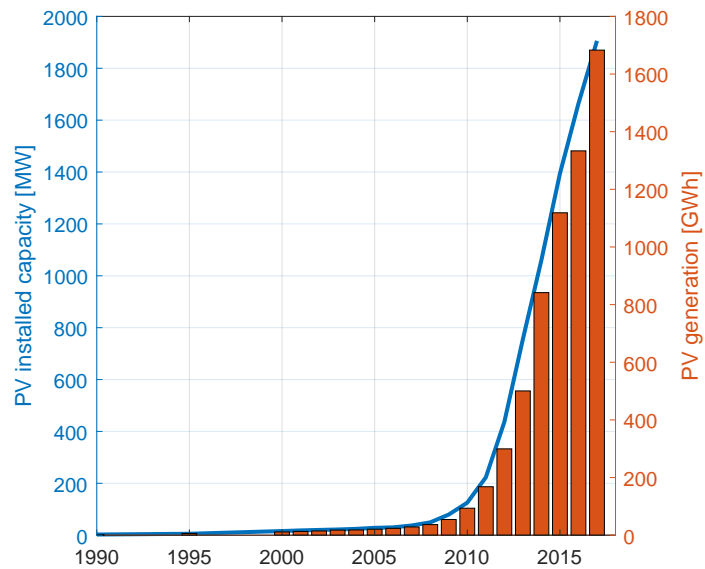


Figure 3: Development of the PV capacity and annual generation between 1990 and 2017 in Switzerland[11]

2.2. Research question

As confirmed by the previous analysis of the reference system [9], the development of the regional renewable energy potential is held back by three factors:

- the lack of exploitation of more than 90% of the PV potential on the roof of buildings
- the under-development of district heating and cooling to distribute renewable resources (geothermal, lake or river resources) in the vicinity of the high density city center
- the lack of strategy for the integration of gas and biogas energy

Unlocking the untapped renewable energy potential requires a large scale deployment of decentralized power generation and heat pumps technologies which are expected to increase the stress on the electricity network while pushing the development of co-generation and district heating and cooling (DHC) networks. At the grid level, the uncertainty in energy generation from renewable energy, the trend towards decentralisation and the emergence of new energy prosumers are going to increase bi-directional energy interconnections [3], therefore challenging the energy networks to balance supply and demand.

In this context, the JA-RED partners are aiming to develop methods to define guidelines for the planning of future multi-energy systems in order to identify actions and opportunities for the implementation of the Swiss Energy Strategy at the regional level. This necessitates to address the following research questions:

- How to define optimal energy transition scenarios ?
- What is the trend between investment and operation cost as a function of the energy transition scenarios ?
- What is the degree of self-sufficiency and self-consumption as a function of the penetration of renewable technology ?
- How to quantify the load shifting potential as a function of the evolution of the grid ?
- To which extent can modern building energy systems provide any flexibility to distribution system operators ?
- What is the hosting capacity of renewable technologies in the grid ?
- How to address the grid operation bottlenecks ?
- Where to invest in smart grid and where are the target region and users ?

Answering these questions requires a multi-disciplinary approach combining competences in urban energy system analysis, multi-period pinch analysis and process integration, thermal and power network modelling, power to gas integration, mobility integration, decision making through data visualisation and in the development of strategic market and business plan.

2.3. Novelty of the proposed solutions compared to the state-of-art

Visual Decision making tool

The innovative combination of public data with energy and network models in a Geographical information system (GIS) has found use as a valuable communication and decision making tool for the REel Demonstrator Community.

Electricity demand profiles allocation

To compensate for the lack of real measurements at building level, a demand profiles allocation model has been developed. The latter consists of a two-stage optimization. In our case, the sum of all the profiles is as close as possible to the profile at the transformer measured by Depsys.

Influence of photovoltaic panel orientation

A method has been developed to evaluate the potential of photovoltaic (PV) panel taking into account the roof availability and orientation of the thousands of roofs found at the city scale, non-flat roofs have been clustered according to their orientation. In the end, each roof is associated with a set of PV generation profiles and corresponding cost and footprint [7].

Load shifting potential assessment

A new metric has been introduced allowing to compare the load shifting potential at the supply-side (integration of PV panels), demand-side (customer behaviour), technical level (integration of heat pump, thermal and electrical storage) and operational level (use of model predictive control). The load shifting potential has been expressed as an equivalent “virtual storage capacity” representing the difference between the initial load and the shifted load[12].

2.4. Description of the deliverable

Based on the analysis of the reference case [9], this report applies and value models developed at the PVLAB-EPFL and IPESE-EPFL in order to assess the impact of distributed generation and ancillary services on the Romande Energie ELeetric power grids. The models are used to evaluate solutions capable of providing flexibility to the power system, meaning

“the capability of a power system to cope with the variability and uncertainty that variable renewable energy generation introduces into the system in different time scales, avoiding curtailment of variable renewable energy and reliably supplying all the demanded energy to customers” [4]

In a first step, competencies developed in the reconstruction of load profiles have been applied to evaluate the energy flow to the grid with sufficient precision. This involves assessments

of profiles for PV generation considering the optimal roofs area and orientation (§4.1) and the allocation of uncontrollable load based on real aggregated measurement (§4.2).

In a second step, the load shifting potential has been evaluated against the consumers behaviour (§4.4), the technical and operational flexibility (§4.4). The assessment of the latest relies on a model generating optimal design and operation of energy technologies in buildings (§4.3 p.21).

For comparison purposes, the load shifting potential has been expressed as an equivalent “virtual” storage capacity, therefore defining a new metric for the evaluation of the flexibility reserve available at the supply-side (integration of PV panels), demand-side (customer behaviour), technical (heat electrification using heat pump, thermal and electrical storage) and operational (Model Predictive Control) level.

Finally, the limits imposed by the existing power supply infrastructure have been identified using a power flow algorithm to detect the bottlenecks in the power grid (§4.5, p.35).

3. Achievement of Deliverable

3.1. Date

This deliverable is handed in April 2019.

3.2. Demonstration of the Deliverable

The deliverable capitalizes on previously research developments of IPESE-EPFL, PVLAB-EPFL and HSLU to identify energy transition guidelines as a function of the evolution of the REel-Demo energy grid, providing material for other project partners to elaborate investment schedule and business models for the future development of the Swiss electrical infrastructure.

Decision making support

On a practical level, the database compiled by the JA-RED partners[9], have been converted into an essential tool to support communication and strategic decisions among the REel Demonstrator Community (Figure 4). The tool allows to visually inspect, at an early stage of the REel Demonstrator, the degree of technical flexibility for the various district's zones, therefore orienting the development of smart grids towards potential users.



Figure 4: Application of the JA-RED database to support decision making among the REel demonstrator Community (Source: Romande Energie, 2018-2019)

Electricity demand profiles allocation

The developed demand profiles allocation model compensate for the lack of real measurements at the building scale, thus allowing to get a realistic estimation of the electricity demand profiles required for multi-energy grid planning analysis.

Optimisation of the PV potential at the district scale

Another improvement for the REel grid evaluation is to consider for each building individually its proper PV potential and corresponding PV generation profile that depends on the roof's area and orientation.

Power grid flexibility assessment

The proposed approach based on the definition of an equivalent virtual battery and of the use of power flow simulation allows to evaluate the capacity and the additional cost of modern building energy systems to provide flexibility to distribution system operators.

3.4. Impact

Besides the actual application of the research topics on the demonstrator that will be extended beyond the end of the project, the impact of this project is to provide methods and information to other project partners for the elaboration of investment schedule and business models and thus further influence the decisions for upcoming investment for renewable en-ergy integration in Switzerland.

For instance, the combination geographical data with modelling results has found use as a valuable decision making tool for the REel Demonstrator Community. Proper visualisation and interpretation of the data are for example boosting the development of the "Solar Garden"¹, where rooftops are mutualised and the smartgrid used to collect and distribute local renewable energy to the Community.

¹<https://jardinsolaire.ch/projet>

4. Research methodology

This section presents the research methodology and approaches to quantify flexibility in a distribution grid whose results are presented in section 5. The generation of the PV profiles are details in section 4.1 and the electricity demand profiles in section 4.2. The improvements in the optimization of the building multi-energy systems is detailed in section 4.3. Sections 4.4 and 4.4 introduce the approaches to evaluate the behavioural and technical flexibility respectively. Last section 4.5 presents the evaluated compliance limits for the grid stability assessment.

4.1. Optimisation of the PV potential

One of the improvement on multi-energy system MILP optimization is to consider for each building individually its proper PV potential and corresponding PV generation profile that depends on the roofs area and orientation. This section presents how these PV profiles have been generated at the city scale starting with the *solar roof*² dataset.

Solar Roof post-processing

The solar roof dataset gives for each roof, its properties (area, orientation) and corresponding building via the building ID (EGID). Using the raw data, it was observed that the aggregated photovoltaic potential at the building or injection point level appeared sometimes to be null. This doesn't come from unreferenced roofs but is the consequence that some roofs cover multiple buildings but are linked to only one EGID. For instance, figure 5 shows the case of two roofs covering two buildings part of a terraced house. Since both roofs have the EGID of the building on the right, the PV potential for the building on the left is null.

²<http://www.uvek-gis.admin.ch/BFE/sonnendach/>

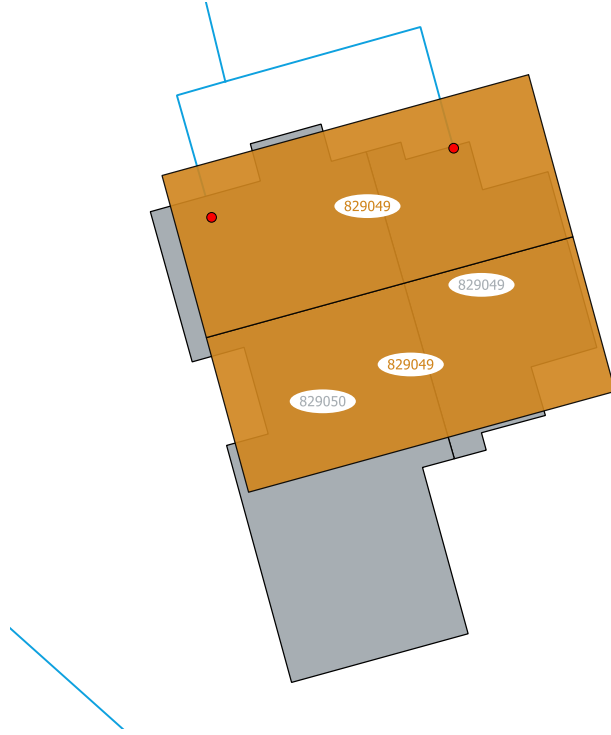


Figure 5: For this terraced house, both roofs (orange) of the original solar roof dataset have the same EGID (829049).

To avoid this situation that has a non negligible impact on metrics such as the mean PV self-consumption ratio at the grid level, all roofs have been reallocated based on their intersection with the building footprints. Keeping only the roofs/buildings intersections is not an option since not many roofs exceed the building edges, as in figure 5. Thus the part of roof R_i allocated to building B_j is $a_{ij} \in [0, 1]$ defined as

$$a_{ij} = \frac{R_i \cap B_j}{\sum_k (R_i \cap B_k)} \quad (1)$$

Where $R_i \cap B_j$ is the intersection area between roof R_i and building B_j . In the case where $\sum_k (R_i \cap B_k) = 0$ meaning that roof R_i has no intersection with any building, then $a_{ij} = a_{mj}$ where R_m is the closest roof (euclidean distance between centroids).

In this way, all buildings of the reference system have at least one roof. Moreover it also allocate to building roofs whose EGID were missing.

Roofs clustering

The MILP building multi-energy optimization required normalized (W/m^2) PV profiles. For a given building, each roof has at least one associated PV profile. For a roof with a tilt angle higher than 5° , the PV modules are assumed to be installed with the roof orientation and only one PV profile is associated with the roof. For flat roofs (tilt $< 5^\circ$), eight configurations and

corresponding profiles have been generated. PV modules can be oriented to the south with a tilt angle between 0 and 60° by step of 10° or in a east-west configuration with a tilt angle of 10°. In this case, the optimization will select one among the eight PV profiles associated with the roof.

Each configuration has a different footprint that depends on the tilt angle in order to consider the inter modules shadowing. For south oriented configuration the distance between two rows of modules is given by the equation 2.

$$D = H \cdot \frac{\sin(\alpha + \beta)}{\sin(\beta)} \quad (2)$$

where H is the module height, α the module tilt and β is minimum sun elevation to avoid shadowing, which is by default 20° corresponding to the sun elevation at noon during winter in Switzerland.

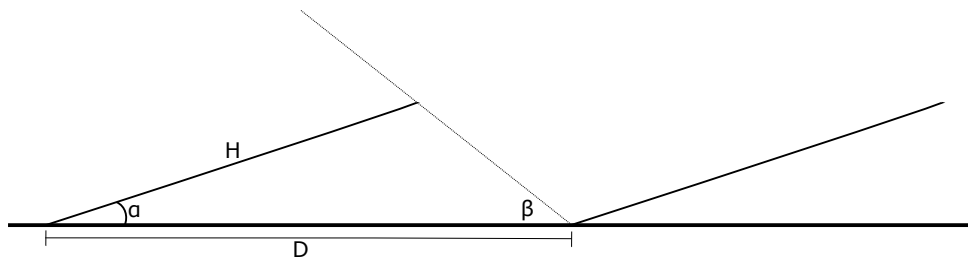


Figure 6: Distance D between two modules for a given module height H , tilt angle α and sun elevation β

In order to avoid generating one PV profile for each roof which can represent thousands of profiles at the city scale, non flat roofs have been clustered according to their orientation (azimuth and tilt). One PV profile is generated for the cluster centroid and associated to each roof of the cluster. Figure 7 shows the classification of about 14k roofs from the city of Rolle and surrounding in 40 clusters.

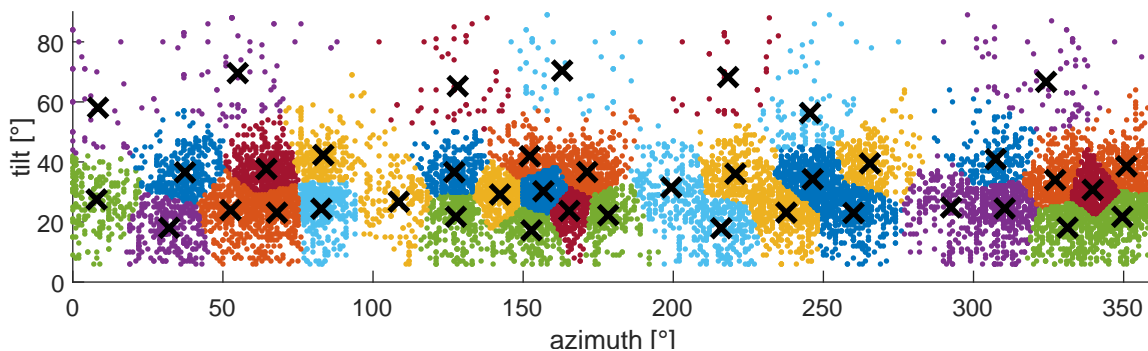


Figure 7: 14'000 roofs from the city of Rolle and surrounding classified in 40 clusters according to their orientation.

Using the cluster centroid instead of the real roof orientation causes an error on the simulated daily power distribution and annual energy production. As regards the latter, figure 8 shows that the average relative error on the annual energy production is below 2.5% for a classification with 40 clusters.

$$\text{error} = \frac{1}{N} \sum_{i=1}^N \frac{|E_r(i) - E_c(c(i))|}{E_r(i)} \quad (3)$$

where N is the number of roofs randomly selected among the 14k roofs, E_r is the roof annual energy production, E_c the annual energy production for the centroid and $c(i)$ define the centroid of cluster in which roof i has been classified.

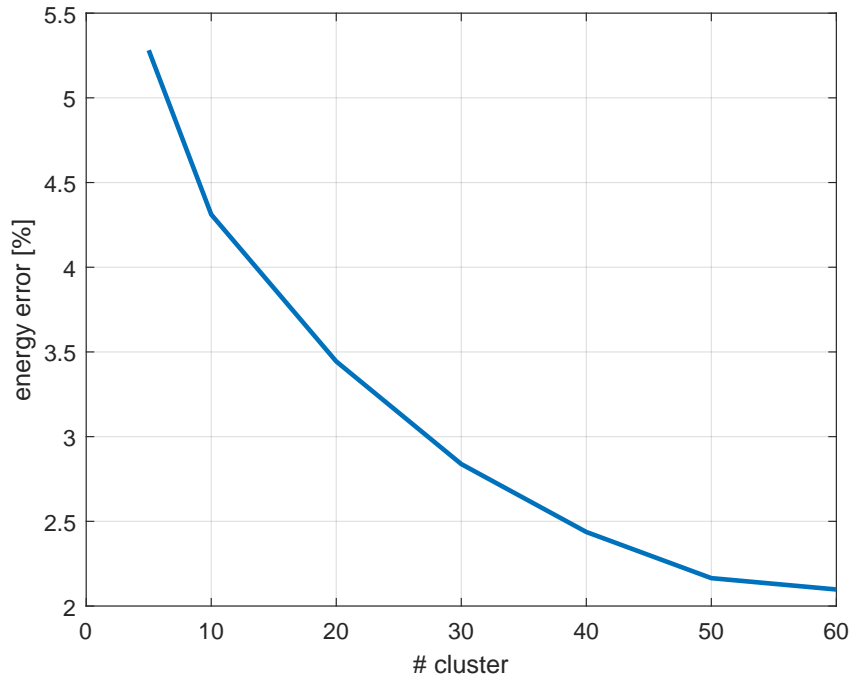


Figure 8: Average of the absolute relative error on the annual energy production between the cluster centroids and 1000 random roofs.

4.2. Load profiles allocation model

In order to assess the impact of distributed generation and ancillary services on distribution grids, the following general data are required.

- grid topology
- building cadastre
- weather conditions
- electric and heat demands

Whereas the three first elements can be found for most distribution grids in Switzerland, both electric and heat demands profiles are rarely available. As regards the electricity consumption, a few Distribution System Operator (DSO) have already replaced conventional meter by smart meters measuring the load at the resolution of 15min. However such data are not available for the reference system (TR3716). Moreover, the use the standard profile (SIA) is not a viable option since the profile aggregated at the level of a distribution grid presents huge peaks due to the lack of stochasticity.

Synthetic load profiles can be emulated, for example using Monte Carlo simulation [1]. Here the approach is to take advantage of the existence of a sufficiently large dataset of load profiles obtained throughout the FLEXI project. The developed method consists of a two-stage optimization. In the first phase a load profile is allocated to each meter, then all profiles are tuned in the second phase to match with potential additional measurements. In our case, the sum of all the profiles should be as close as possible to the profile at the transformer measured by Depsys.

First stage optimization

The overall idea of the first stage optimization problem is to consider the grid as a directed graph, formed by a set of nodes N , among which, the set $N_L \subset N$ of nodes has unknown load profiles. Additionally, the set $N_K \subset N$ contains measured load profiles. The root node (or transformer) is denoted the $N_P \subset N$. The reference dataset of load profiles is considered as virtual nodes J . Any load profile is assumed to be measured on the same time-span T . Finally, for each node $n \in N_L$ and $j \in J$ we define a building category $h_n \subset H$. The various sets are described in table 1. The problem can be defined as connecting each node in N_L to one single node in J such that the difference between the allocated annual energy of the reference load profile, E_n^{VAR} , and the one from the meter (assumed to be known for every node), E_j^{REF} , is smaller than a given tolerance ϵ_E . Moreover the building category of the reference load profile should match with the building category associated to the meter.

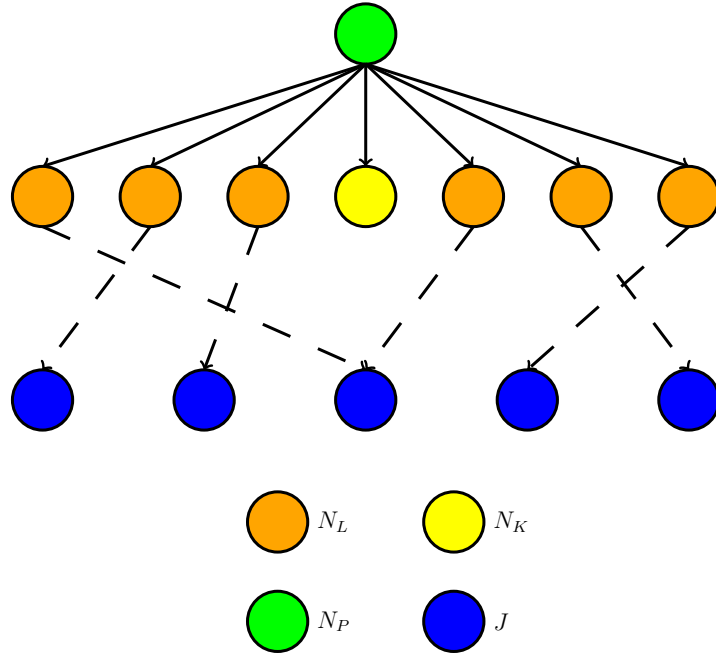


Figure 9: Illustration of the first stage allocation.

Table 1: Networks topology and sets

| Set | Subset of | Description |
|-------|-----------|--|
| N | - | nodes |
| N_P | N | single root node with available load profiles |
| N_L | N | nodes with unknown load profiles |
| N_K | N | nodes with known load profiles |
| J | N | virtual nodes representing available load profiles |
| T | - | time |
| H | - | building type |

As pictured in figure 9, it is possible that a single reference load profile is allocated to more than one node in N_L . In general, a parameter of the optimization problem is defined as the maximum number of allocation for each building category max_{alloc}^h . The other parameters of this first stage are described in the following table.

Table 2: Parameters

| Variable | Set | Subset | Unit | Description |
|--------------------|----------------|----------------------------|------|---|
| E_n^{REF} | \mathbb{R}_+ | $\forall n \in N_L$ | J | measured annual consumption |
| h_n | H | $\forall n \in N_L \cup J$ | (-) | building category |
| max_{alloc}^h | \mathbb{N}_+ | $\forall h \in H$ | (-) | maximum allocation of a load per category |
| ϵ_E | $[0, 1]$ | | (-) | relative tolerance on energy |

Finally, the decision variables of the first stage optimization are the annual consumption of the allocated load profile, E_n^{ORG} , the final annual energy consumption of the allocated load profile, E_n^{VAR} , the allocation and normalization matrix, $\alpha_{n,j}$ and $\beta_{n,j}$. The allocation matrix is defined such that $\alpha_{n,j} = 1$ if the load j is allocated at the node n . In order to integrate the constraints on the building category in the design of the optimization, it is necessary to define these decision variables only on the appropriate domain. Indeed, we know before-hands that $\alpha_{n,j} = 0$ if $h_n \neq h_j$. Hence α and β are defined only for the subset $\bigcup_{h \in H} \{(n, j) | n \in N_L^h \wedge j \in J^h\}$, where N_L^h and J^h are the subset of the meters and the reference load profiles per building category.

Table 3: Decision variables - first optimization

| Variable | Set | Subset | Unit | Description |
|--------------------|----------------|---|------|---|
| E_n^{ORG} | \mathbb{R}_+ | $\forall n \in N_L$ | J | original annual loads allocated to node n |
| E_n^{VAR} | \mathbb{R}_+ | $\forall n \in N_L$ | J | annual loads allocated to node n |
| $\beta_{n,j}$ | \mathbb{R}_+ | $\bigcup_{h \in H} \{(n, j) n \in N_L^h \wedge j \in J^h\}$ | (-) | normalization ratio |
| $\alpha_{n,j}$ | $[0, 1]$ | $\bigcup_{h \in H} \{(n, j) n \in N_L^h \wedge j \in J^h\}$ | (-) | allocation variable |

The objective of this first optimization is to minimize the difference between the original annual load and the allocated one.

$$\text{minimize } \sum_{n \in N_L} (E_n^{\text{ORG}})^2 - 2 \cdot E_n^{\text{ORG}} \cdot E_n^{\text{VAR}} + (E_n^{\text{VAR}})^2 \quad (4)$$

The allocated annual load is defined as the reference load times the normalization matrix

$$\forall h \in H, \quad E_n^{\text{VAR}} = \sum_{j \in J^h} \beta_{n,j} E_j^{\text{REF}} \quad \forall n \in N_L^h \quad (5)$$

The original annual load is simply defined as the reference annual load allocated in node n

$$E_n^{\text{ORG}} = \sum_{j \in J} \alpha_{n,j} E_j^{\text{REF}} \quad \forall n \in N_L \quad (6)$$

The following constraints ensure that only one load from the reference dataset is allocated to a meter in the network

$$\forall h \in H, \quad \sum_{j \in J^h} \alpha_{n,j} = 1 \quad \forall n \in N_L^h \quad (7)$$

However, each load from the reference dataset can be used up to a pre-defined number of times.

$$\forall h \in H, \quad \sum_{n \in N_L} \alpha_{n,j} \leq \max_{alloc}^h \quad \forall j \in J_h \quad (8)$$

The relation between the connectivity matrix α (where all elements are either 1 or 0) and the normalization matrix β is defined as follow.

$$\forall h \in H, \quad \alpha_{n,j} = \begin{cases} 0, & \text{if } \beta_{n,j} = 0 \\ 1, & \text{otherwise} \end{cases} \quad \forall n \in N_L^h, j \in J^h \quad (9)$$

The constraint on the annual energy error is defined as:

$$1 - \frac{2 \cdot E_n^{VAR}}{E_n^{REF}} + \frac{(E_n^{VAR})^2}{(E_n^{REF})^2} \leq \epsilon_E^2 \quad \forall n \in N_L \quad (10)$$

Second stage optimization

The aim of the second optimization is to tune the allocated load profiles in order to match the resulting power profile at the transformer node, $P_{N_P,t}^{VAR}$ with the measured one $P_{N_P,t}^{REF}$, i.e having the relative difference between both under a given tolerance ϵ_P . For this, a tuning matrix defined as $\beta_{n,t}$ can deform any allocated load profile $P_{n,t}^{ORG}$. Additionally, the constraints on the annual energy consumption still apply. The decision variables are defined in table 4.

The original load profile from the reference dataset allocated to the specific node n is extracted with the help of the allocation matrix α from the previous stage as follow.

$$P_{n,t}^{ORG} = \sum_{j \in J} \alpha_{n,j} P_{j,t}^{REF} \quad \forall n \in N_L, t \in T \quad (11)$$

Table 4: Decision variables - second optimization

| Variable | Set | Subset | Unit | Description |
|-----------------|----------------|---|------|---------------------|
| $P_{n,t}^{VAR}$ | \mathbb{R}_+ | $\forall n \in N_L \cup N_P, \forall t \in T$ | W | load profiles |
| E_n^{VAR} | \mathbb{R}_+ | $\forall n \in N_L$ | kWh | annual loads |
| $\beta_{n,t}$ | \mathbb{R}_+ | $\forall n \in N_L, \forall t \in T$ | (-) | normalization ratio |

The additional optimization parameters are defined in table 5.

Table 5: Parameters - second optimization

| Variable | Set | Subset | Unit | Description |
|------------------------|----------------|---|------|------------------------------------|
| $P_{n,t}^{\text{ORG}}$ | \mathbb{R}_+ | $\forall n \in N_L \cup N_P, \forall t \in T$ | W | originally allocated load profiles |
| $P_{n,t}^{\text{REF}}$ | \mathbb{R}_+ | $\forall n \in N_P, t \in T$ | W | measured load |
| ϵ_P | $[0, 1]$ | | (-) | relative tolerance on power |
| ϵ_E | $[0, 1]$ | | (-) | relative tolerance on energy |
| TS_t | \mathbb{R}_+ | $\forall t \in T$ | s | timestep |

The idea is to match a given power profile measurement without deforming too much the load profiles. For that, the difference between the allocated load P_n^{VAR} and the original one $P_{n,t}^{\text{ORG}}$ is set as the objective function.

$$\text{minimize } \sum_{n \in N_L} \sum_{t \in T} 1 - \frac{2 \cdot P_n^{\text{VAR}}}{P_{n,t}^{\text{ORG}}} + \frac{(P_{n,t}^{\text{VAR}})^2}{(P_{n,t}^{\text{ORG}})^2} \quad (12)$$

The final allocated load $P_{n,t}^{\text{VAR}}$ is the original load tuned by the $\beta_{n,t}$ variable.

$$P_{n,t}^{\text{VAR}} = \beta_{n,t} P_{n,t}^{\text{ORG}} \quad \forall n \in N_L, \forall t \in T \quad (13)$$

The resulting load profile at the root node can be expressed as

$$P_{n,t}^{\text{VAR}} = \sum_{m \in N_L} P_{m,t}^{\text{VAR}} + \sum_{m \in N_K} P_{m,t}^{\text{REF}} \quad \forall n \in N_P, \forall t \in T \quad (14)$$

The annual energy consumption at each node is updated by adding the following constraints (noting the change of unit to convert Ws to kWh):

$$E_n^{\text{VAR}} = \sum_{t \in T} P_{n,t}^{\text{VAR}} \cdot \text{TS}_t / 3.6 \cdot 10^6 \quad \forall n \in N_L \quad (15)$$

Similar to the first stage, a constraint on the annual energy consumption is maintained.

$$1 - \frac{2 \cdot E_n^{\text{VAR}}}{E_n^{\text{REF}}} + \frac{(E_n^{\text{VAR}})^2}{(E_n^{\text{REF}})^2} \leq \epsilon_E^2 \quad \forall n \in N_L \quad (16)$$

Finally, the resulting power profile at the root node must be close to the measured power profile at the root node to a given precision

$$1 - \frac{2 \cdot P_{n,t}^{\text{VAR}}}{P_{n,t}^{\text{REF}}} + \frac{(P_{n,t}^{\text{VAR}})^2}{(P_{n,t}^{\text{REF}})^2} \leq \epsilon_P^2 \quad \forall n \in N_P, \forall t \in T \quad (17)$$

Combining both optimization allows to get a representative state model of the network loads, and enable further studies.

4.3. Building multi-energy optimisation

A model for the optimal design and operation of the energy technologies as a function of the energy demand and subject on investment constraints as been developed by [16, 8]. The challenge has been to provide a computation method providing both the conceptual design and the yearly load scheduling with sufficient precision in a reasonable computing time of a few seconds.

The model therefore implements:

- an optimal operation strategy to provide comfort (heating, cooling and electricity) in the buildings using appropriate temperature level;
- hourly time steps to provide sufficient accuracy;
- part-load efficiencies, start-up and shutdown of the equipment;
- centralized and decentralized energy technologies;
- thermal and electrical storage;
- thermal mass of the buildings as heat storage with variable indoor temperature;
- straightforward integration of additional energy sink, source or storage such as power to gas; (P2G), gas to power (G2P), residual heat source and energy storage.

Moreover, recently improvements includes the placement and orientation of PV on roof of buildings considering shading effects (§4.1)

The proposed method generates various conceptual design (scenario) of the urban energy system, without going into the detail of the energy network's topology, using process integration and multi-objective optimization techniques. The method is characterized by the use of:

- multi-objective parametric optimization of a MILP formulation for the process integration;
- a two-level decomposition of the problem at building and district scale;
- building energy system (BES) integrated as a meta-model at district scale;
- spatial, temporal and typological data reduction techniques;
- cyclic constraints for thermal and electrical storage;
- piece-wise linearization for efficiencies and distribution temperatures.

The generated alternatives are compared with key performance indicators such as CAPEX and OPEX as a function of the sizes and operation of centralized and decentralized energy conversion equipment.

Temporal data reduction

A k-medoids clustering method is performed to decrease the temporal input data of the problem from 8760 hours hourly DRY profile to 6 to 12 × 24 hours typical operating periods with,

in addition, 2 extreme periods to reflect peak demand hours. Two independent variables have been used: the daily ambient temperature and the global solar irradiance. Further information on the applied approach are given in [13] and [15]. Table 6 provides the selected days and annual frequency of occurrence which allow, as an initial approach, to extract the clustered load curves from the original DRY profiles.

Table 6: Temporal cluster center and occurrence for climate zone Geneva- Cointrin

| Period | Day | Date | Frequency |
|---------------|------------|-------------|------------------|
| 1 | 264 | 21.09. | 54 |
| 2 | 59 | 28.02. | 46 |
| 3 | 222 | 10.08 | 17 |
| 4 | 72 | 13.03. | 49 |
| 5 | 206 | 25.07. | 52 |
| 6 | 7 | 07.01. | 68 |
| 7 | 254 | 11.09. | 49 |
| 8 | 169 | 18.06. | 30 |

Main constraints of the MILP multi- objective building model

The modeling framework relies on MILP techniques to describe both the continuous (e.g. output modulation) and logical (e.g. start-up) behaviour of the devices. An overview of the latter is illustrated in figure 10; it comprises an air-water heat pump as well as electric auxiliary heaters to satisfy the different heating requirements. Energy is stored in either stationary batteries, the domestic hot water and buffer tanks or the building envelope. Photovoltaic and solar collector panels act as renewable energy sources, the latter being only connected to the domestic hot water tank in regard to the strong seasonal disparity of generation potential and space heating demand. The different energy systems are finally interconnected through the main energy distribution networks: the natural gas, electricity and fresh water grid. The figure solely illustrates an air–water heat pump as primary thermal conversion unit, as it is the only unit considered in this study. However, it is also possible to integrate a cogeneration heat plant (CHP) device, solid oxide (SOFC), and low temperature proton exchange membrane fuel cells (LPPEM). In addition, it is worth noting that the final hydraulic layout (including, e.g., pumps, by-passes, three-way valves) of the designed BES may be implemented differently, according to the selected solution. Further details on the optimization problem formulation and input data are reported in [16].

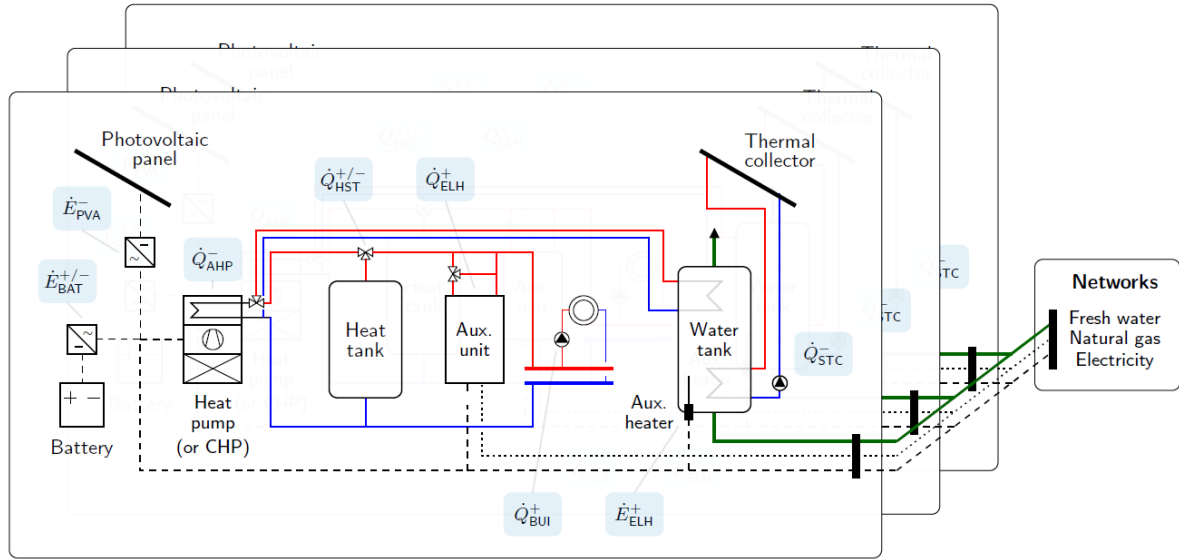


Figure 10: Building energy system structure and the respective control variables (blue)

The optimal integration of the building energy technologies is formulated as a multi-objective optimization problem based on a MILP formulation. The sets and their respective indices used in the following are reported in Table 7.

Table 7: List of defined sets with description

| Set | Index | Increment | Cyclic | Description |
|----------|-------|-----------|--------|----------------------------|
| P | p | dp | No | Period (day) |
| T | t | dt | Yes | Time (hour) |
| K | k | | No | Temperature level |
| U | u | | | Utility types |
| B | b | | | Building |
| S | s | | | Surface of Building |
| C | c | | | Configuration of PV Panels |

Objectives

The main objective is the annual building operating expenses (OPEX). The OPEX comprise both the natural gas and power grid exchanges. The former are defined in Equation (18) where (op) refers to the grid energy tariffs, (E) to the electrical power flows, (H) to the chemical–natural gas–power flows, (d) to the indexed time step duration, and (Σ) to the set of decision variables

reported in [14].

$$\min_{\Sigma} \sum_{p=1}^P \sum_{t=1}^T \left(\dot{Q}_{grid,p,t}^+ \cdot op_{p,t}^{th,+} + \dot{E}_{grid,p,t}^+ \cdot op_{p,t}^{el,+} - \dot{E}_{grid,p,t}^- \cdot op_{p,t}^{el,-} + \dot{H}_{grid,p,t}^+ \cdot op_{p,t}^{ng,+} \right) \cdot d_p \cdot d_t \quad (18)$$

The second objective, formulated as a parametric ϵ -constraint in the optimization problem, is the present capital expenses related to the different unit purchases over the project horizon (N). In Equation (19), ($I_{1,u}$) and ($I_{2,u}$) denote the linear cost function parameters, (y_u) the unit existence while (f_u) is the device sizing variable. In addition, (N_u) refers to the unit lifetime, (r) the project interest rate and (rep_u) to the number of unit replacements over the project horizon.

$$\sum_{u=1}^U (I_{1,u} \cdot y_u + I_{2,u} \cdot f_u) + \sum_{u=1}^U \sum_{n=1}^{rep_{u,N}} \frac{1}{(1+r)^{n \cdot N_u}} \cdot (I_{1,u} \cdot y_u + I_{2,u} \cdot f_u) \leq \epsilon_I \quad (19)$$

Finally, a third objective function implemented as an *epsilon*-constraint is used to represent the power network constraint: the grid multiple (GM). As detailed in Equation (20), this parameter limits the building power profile peaks (\dot{E}_{grid}) with respect to the daily average demand and thus decreases the consequent stress on the distribution network from strong demand/supply surges. For the sake of readability, the total period duration is denoted by (n_t).

$$\frac{\left(\dot{E}_{grid,p,t}^+ - \dot{E}_{grid,p,t}^- \right)}{\frac{1}{n_t} \sum_{t=1}^T \left(\dot{E}_{grid,p,t}^+ - \dot{E}_{grid,p,t}^- \right)} \leq \epsilon_{GM} \quad (20)$$

Heat Cascade

The heat cascade balances the system heat loads while satisfy the second law of thermodynamics. Equation (21) thus defines the thermal energy balance of each temperature interval k where ($Q_{u_h,k}^-$) represents the released heat of utility (u_h), ($Q_{u_c,k}^+$) represents the heat demand of utility (u_c), and (R_k) the residual heat cascaded to next interval ($k+1$). In addition, no heat is cascaded at the first and last intervals to ensure a closed thermal energy balance.

$$\begin{aligned} \dot{R}_{k,p,t} - \dot{R}_{k+1,p,t} &= \sum_{u_h=1}^U \dot{Q}_{u_h,k,p,t}^- - \sum_{u_c=1}^U \dot{Q}_{u_c,k,p,t}^+ \\ \dot{R}_{1,p,t} &= \dot{R}_{n_k+1,p,t} \end{aligned} \quad \forall p \in \mathbf{P}, t \in \mathbf{T}, k \in \mathbf{K} \quad (21)$$

Energy Balances

The electrical and natural gas energy balances are defined in Equation (22) where (E_{build}^-) refers to the building uncontrollable load profile.

$$\begin{aligned} \dot{E}_{grid,p,t}^+ + \sum_{u=1}^U \dot{E}_{u,p,t}^+ &= \dot{E}_{grid,p,t}^- + \sum_{u=1}^U \dot{E}_{u,p,t}^- + \dot{E}_{b,p,t}^- \\ \dot{H}_{grid,p,t}^+ &= \sum_{u=1}^U \dot{H}_{u,p,t}^- \end{aligned} \quad \forall p \in \mathbf{P}, t \in \mathbf{T} \quad (22)$$

Cyclic Conditions

To prevent any energy accumulation between the different independent operating periods (p), cyclic constraints of Equation (23) enforce all system states to return to their initial value at the end of each control horizon (n_t). The latter constraints target the dwelling temperature (T_b) as well as the thermal (Q) and electrical energy (E) stored in the respective storage units. The typical days (p) represent indeed different operating conditions with a given probability of occurrence during the system lifetime. Equation (23) is therefore included in the problem formulation to avoid any energy bias.

$$\begin{aligned} T_{b,p,1} &= T_{b,p,n_t} \\ Q_{u,p,1} &= Q_{u,p,n_t} \\ E_{u,p,1} &= E_{u,p,n_t} \end{aligned} \quad \forall p \in \mathbf{P}, u \in \mathbf{U} \quad (23)$$

Unit Sizes

The unit existence (y_u) and logical state on/off ($y_{u,p,t}$) are expressed in equation (23) where (F_u^{min}) and (F_u^{max}) describe the device minimal and maximal sizing values.

$$\begin{aligned} y_u \cdot F_u^{min} &\leq f_u \leq y_u \cdot F_u^{max} \\ y_{u,p,t} &\leq y_u \end{aligned} \quad \forall u \in \mathbf{U} \quad (24)$$

Photo-voltaic Panel

One novelty of this report is the inclusion of different orientation of the PV Panels in the city district. For this reason, this specific unit model is discussed further in detail. The unit model of the PV panel is stated by Equations (25). Accordingly, the energy system model additionally consists of the set "Surface" for describing the building's envelope and "Configuration" for describing the different orientation possibilities on this surface. The sizing value f_{PV} is the total area, which is covered with PV panels. The variable n^{PV} is the number of modules, A^{PV} the size of one module. The installation of panels is limited by the available surface area. Thereby, the filling rate ψ is considered to be 70% of the Surface area $A_{b,s}$. Furthermore the footprint β_c respects the shading of the panels to each other at different configurations. The different generated specific electricity \dot{e}^{PV} (see Section 4.1) and the installed Panels of every configuration on every surface give the generated Electricity \dot{E}_{PV}^+ .

$$\begin{aligned}
f_{PV} &= A_{PV} \cdot \sum_s^S \sum_c^C n_{b,s,c}^{PV} & (25) \\
\psi_b \cdot A_{b,s} &\geq A_{PV} \cdot \sum_c^C \beta_c \cdot n_{b,s,c}^{PV} \\
\dot{E}_{PV,b,p,t}^+ &= A_{PV} \cdot \sum_s^S \sum_c^C n_{b,s,c}^{PV} \cdot \dot{e}_{b,s,c,p,t}^{PV} & \forall b \in \mathbf{B}, \forall p \in \mathbf{P}, \forall t \in \mathbf{T}
\end{aligned}$$

4.4. Load shifting

The load shifting potential has been studied at the demand-side (customer behavioural flexibility) and supply-side (integration of PV panels, heat pump, thermal and electrical storage) and at the operational level (use of model predictive control).

Behavioural flexibility

The behavioural flexibility of households has been studied by the mean of a field experiment conducted in the Jura region. The Flexi project consists in proposing an alternative energy tariff to a representative panel of households, customers from the Société des Forces Electriques de La Goule, all equipped with smart meters. The goal of this experiment is to measure the ability of the households to shift their electricity consumption in time as a response to financial incentives. Two separate models are considered, the first consider a fixed low rate period from 11 a.m to 3 p.m. The second is a dynamic tariff considering three possible windows of low rate period:

- From 10 a.m to 1 p.m
- From 1 p.m to 4 p.m
- From 4 p.m to 7 p.m (only during summer time)

The choice of the low rate period is defined based on weather forecasts to match with sunny periods (and possibly high PV generation). A text is sent to the participants of this treatment every day with the "price forecast" for the next day. In both case, in low rate periods the energy tariff is decreased by a bonus 15 cts/kWh with respect to the 27.45cts/kWh flat tariff, while outside of the low rate periods it is increased by 4cts/kWh. This financial incentive has been adjusted such that an average household that makes no change in his behaviour makes no gain of loose over a full year.

The participants were recruited along three different waves. For each wave, the number of participants following the first treatment or the second treatment is indicated in table 8. In

addition to the two treatment groups, a control group is defined. No information was given to this group as its purpose is to serve as a reference.

Table 8: # of participants per treatment groups and waves

| Wave | Launch date | Groups | | | Total |
|-------|-------------|-----------|-----------|---------|-----------|
| | | C | T1 | T2 | |
| 1 | 01.07.2016 | 14 (9) | 15 (10) | 15 (10) | 44 (29) |
| 2 | 01.10.2016 | 16 (14) | 16 (12) | 16 (4) | 48 (30) |
| 3 | 01.01.2017 | 253 (192) | 252 (197) | - | 505 (389) |
| Total | | 283 (215) | 283 (217) | 31 (14) | 597 (446) |

The following paragraphs aims at briefly describing how the reaction of the households were measured and how the theoretical potential for flexibility was established.

Practical flexibility

In order to assess the performance of the households with respect to their treatment, two specific metrics are used. The first considers a flexibility score and assess the relative amount of energy consumed in the desired time window. The second metrics is the daily energy consumption.

The flexibility score is defined for each household and each day according to equation 26. This score can be seen as the ratio between the energy consumed during the low rate period and the total energy consumed during the day. In order to accommodate with the fact the low rate periods can be different from day to day (for the second treatment), the score is normalized by the relative duration of this low rate period.

$$S = \frac{E_{\text{flexi}}/E_{\text{day}}}{d_{\text{flexi}}/24h} \quad (26)$$

Where:

- E_{flexi} is the amount of energy consumed during the reduced tariff period, also called a flexi period in the following.
- E_{day} is the amount consumed during the considered day.
- d_{flexi} is the duration of a flexi period (always 4 hours for treatment 1 group but can vary between 3 and 9 hours for the second treatment group. In the case where no flexi period is scheduled for a day, the flexi score is obviously not defined.

These two metrics can be calculated for each treatment group for every day of the experiment. To assess the households' change in behaviour, the relative variations of these metrics

between the period of experiment and a corresponding period before the experiment are evaluated.

Theoretical flexibility

The theoretical behavioural flexibility potential is determined with the help of a dedicated method similar to Non Intrusive Appliance Load Monitoring (NIALM). The goal of the developed method is to deduce, from the power measurement of the smart meters, what kind of appliances were turned on at which time and deduce from this information if the corresponding energy could be shifted or not.

To achieve this, a dedicated methodology was developed. The algorithm disaggregate the whole-house power consumption into eight different categories based either on the type of appliance or on the related activity. Figure 11 presents an example of the output of the disaggregation of a single house for a day.

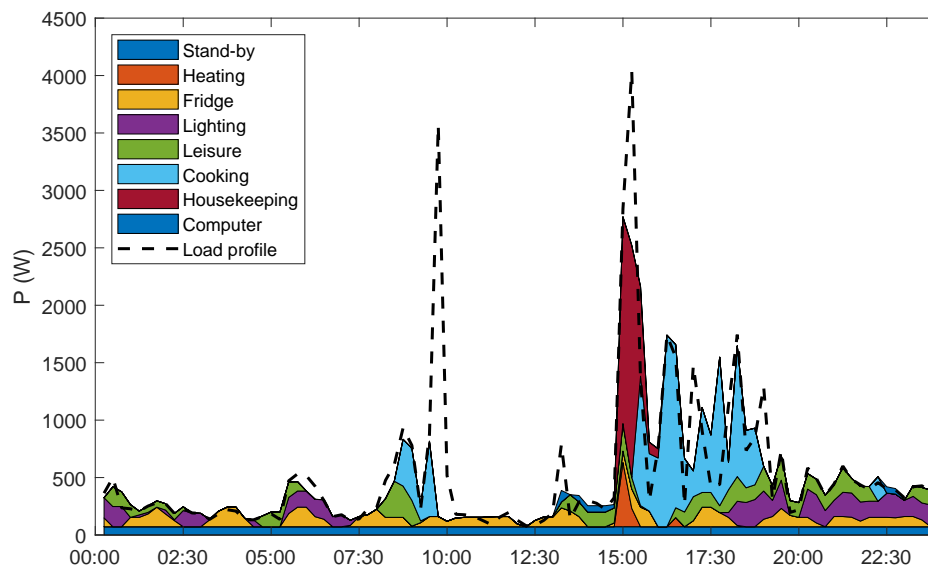


Figure 11: Example of a disaggregated load curve for a single day

The principle of this methodology relies on a statistical approach. For each household, the number of inhabitants, age group of each inhabitant and employment state is collected through a survey. Based on this information, it's possible to generate an activity chain following a Markov process. Then deduce for each activity what appliance can be used using a pseudo-random selection process. The appliances for a given activity are reported in table 9. Additionally, the list of appliances corresponding to a given activity is filtered according to the nominal power of each appliance (reported in table 10) and the available power budget. The power signal for each selected appliance is then generated using the nominal power (re-

ported in table 10) and then aggregated into the eight categories. A general illustration of the methodology is depicted in figure 12.

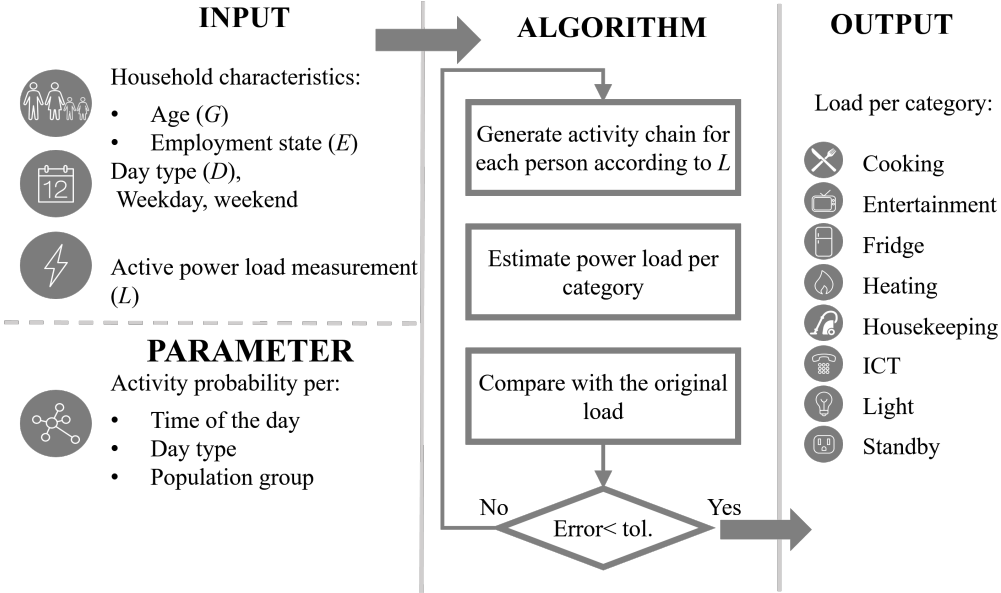


Figure 12: Basic principle of the developed disaggregation methodology

As an example, the share of energy consumed per category is represented as a pie chart on figure 13 and represents the average share across all considered households.

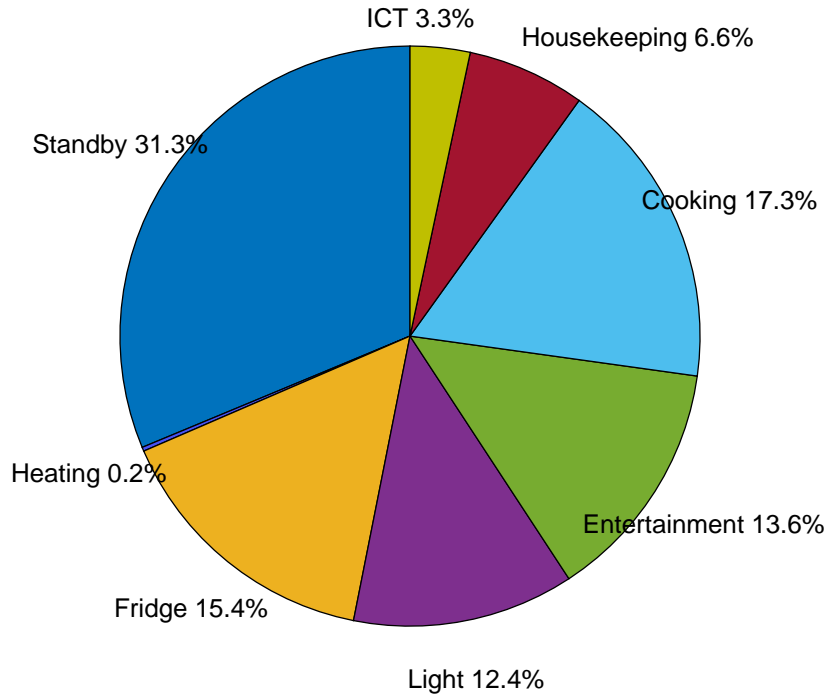


Figure 13: Share of energy consumed per category

Once the disaggregation has been performed it is possible to determine the instantaneous share of shiftable energy by looking at the flexibility potential of each category. Three levels of flexibility potential have been defined as follows:

- Not shiftable
- Hardly shiftable
- Easily shiftable

For each category one of these levels of flexibility has been assigned as reported in table 11. From this consideration, it is possible to define a theoretical flexi score similar to the one of equation 26 as proposed in the following equation:

$$S_{th} = \frac{E_{flexi}^0 + E_{outflexi}^{easy\ shiftable} + E_{outflexi}^{hardly\ shiftable}}{\frac{E_{day}}{24h}} \quad (27)$$

One has to note that the definition of this score relies on the hypothesis that the energy is purely shifted and no energy savings or additional energy needs are derived, the results will, however, show that this hypothesis is not experimentally satisfied. It is hence possible to compare the theoretical flexi score with the practical flexi score calculated in the previous section.

Table 9: List of possible activities and related appliances.

| Activities | Appliances |
|-------------------|---|
| Cleaning | vacuum, TV, stereo, lights |
| Using a computer | TV, stereo, PC, laptop, printer, lights |
| Cooking | stove, oven, microwave, kettle, TV, stereo, lights |
| Washing dishes | dishwasher, TV, stereo, light |
| Eating | coffee maker, microwave, kettle, TV, stereo, lights |
| Do the homework | TV, stereo, PC, printer, laptop, lights |
| Playing a game | TV, stereo, gaming console, lights |
| Laundry | washing machine, tumble dryer, TV, stereo, lights |
| Music | stereo, PC, tablet, laptop, lights |
| Outdoor | ∅ |
| Sleeping | ∅ |
| Watching TV | TV, DVD player, PC, tablet, laptop, lights |
| Showering | hairdryer, TV, stereo, lights |
| Working | ∅ |

Table 10: Appliances and corresponding nominal power grouped per category

| Category | Appliance | P_{Nominal} (W) |
|------------------|----------------------------|--------------------------|
| Cooking | coffee maker | 800 |
| | microwave | 1250 |
| | kettle | 1800 |
| | oven | 2400 |
| | stove | 500 |
| Entertainment | TV | 124 |
| | TV box | 20 |
| | DVD player | 80 |
| | PC | 110 |
| | laptop | 55 |
| | tablet | 7 |
| | stereo | 100 |
| | gaming console | 180 |
| Fridge | fridge (with a freezer) | 94 |
| | fridge (without a freezer) | 66 |
| | freezer alone | 62 |
| Heating | hairdryer | 600 |
| | boiler | 2000 |
| | heat-pump | 1000 |
| Housekeeping | washing machine | 406 |
| | tumble dryer | 2500 |
| | dishwasher | 1131 |
| | vacuum | 2000 |
| ICT ³ | printer | 23 |
| Light | lighting | 137 |
| Standby | modem (and similar) | 8 |

³ICT: Information and Communication technology

Table 11: Potential for load shifting per category

| Categories | Potential |
|---------------|------------------|
| Standby | not shiftable |
| Heating | hardly shiftable |
| Fridge | not shiftable |
| Light | not shiftable |
| Entertainment | hardly shiftable |
| Cooking | not shiftable |
| Housekeeping | easy shiftable |
| ICT | hardly shiftable |

Operational flexibility

In order to quantify various flexibility sources, a metric is proposed [12] which estimate the time dependent profiles of power mismatches ($\Delta \dot{E}_{virtual,p,t}$) considering different electricity prices, for instance flat electricity ($\dot{E}_{grid,p,t}$) price and average day-ahead spot-load ($\dot{E}'_{grid,p,t}$) prices (Figure 14). This leads to the definition of a flexibility demand profile $\Delta \dot{E}_{p,t}$ equivalent to charging and discharging load of virtual battery defined by equation 28.

$$\Delta \dot{E}_{p,t} = \dot{E}_{grid,p,t} - \dot{E}'_{grid,p,t} \quad (28)$$

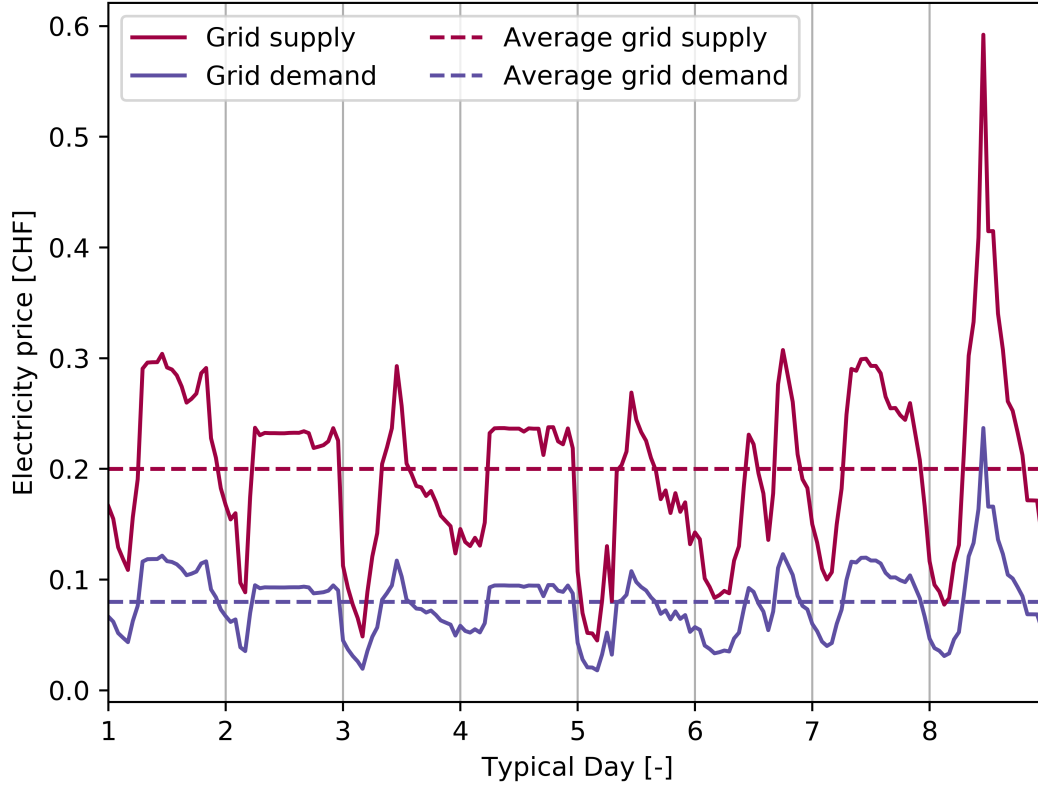


Figure 14: Electricity flat price (dash line) and average spot-load price profiles (continuous line) for each typical days of the year (source: data from EPEX SPOT).

The state of charge (SOC) of the virtual battery is defined by equation 29.

$$SOC_{p,t+1} = SOC_{p,t} + \Delta \dot{E}_{p,t} \cdot d_t \quad (29)$$

The power (F^{pow}), capacity (F^{cap}) and efficiency (η) are defined for each operating period (p) by equations 30-32.

$$F_p^{pow} = \frac{1}{n_t} \sum_{t=1}^{\tau} | \dot{E}'_{grid,p,t} - \dot{E}_{grid,p,t} | \quad \forall p \in \mathbf{P} \quad (30)$$

$$F_p^{cap} = \max_t SOC_{p,t} \quad \forall p \in \mathbf{P} \quad (31)$$

$$\eta_p = \frac{(SOC_{p,1} - SOC_{p,n_t})}{\sum_{t=1}^{\tau} (\Delta \dot{E}_{p,t}^+ \cdot d_t)} \quad \forall p \in \mathbf{P} \quad (32)$$

Figure 15 shows flexibility demand profile and the state of charge (SOC) of the Hopital-TR3716 district. When the spot-load price is lower than the average price (violet) the District is comparatively consuming more electricity and discharges the virtual battery.

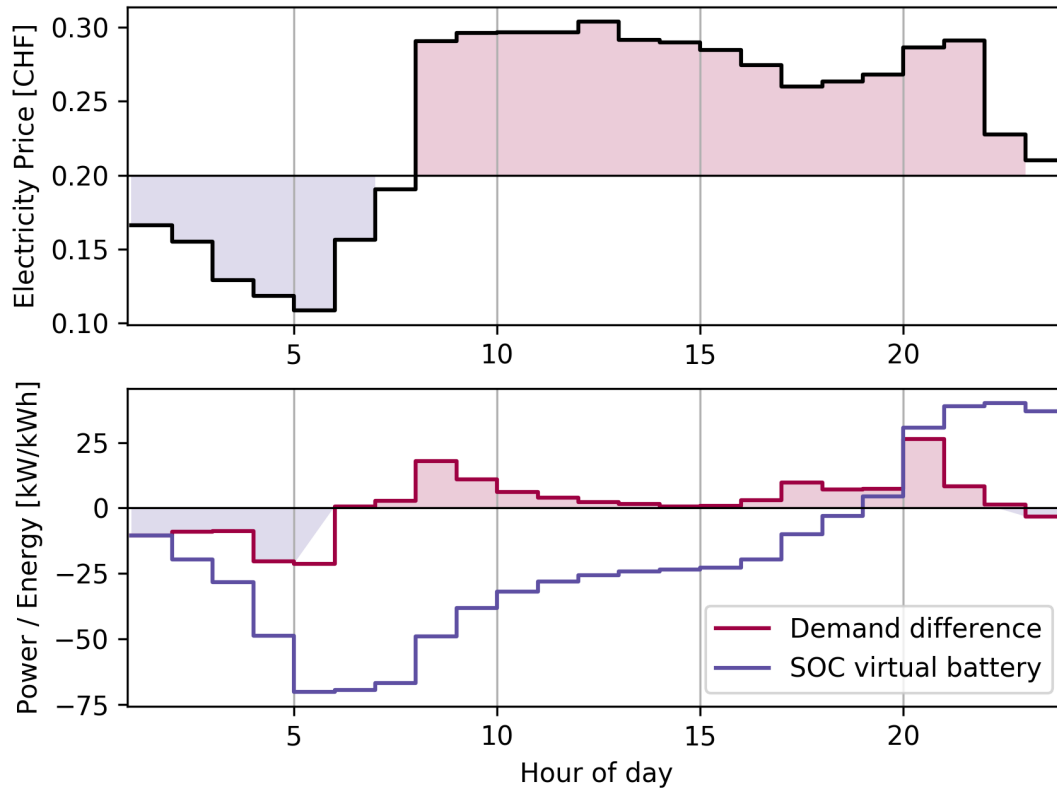


Figure 15: Flexibility demand profile (red) and state of charge (violet) of scenario 2 without grid constraint.

Technical flexibility

The technical flexibility compares the flexibility demand ($\Delta \dot{E}_{s,p,t}$) and ($\Delta \dot{E}_{s',p,t}$) for different investment scenarios (s) and (s').

4.5. Grid stability assessment

To assess the grid stability and operation bottlenecks, the HOPITAL-TR3716 low voltage grid has been modelled using the a power flow solver OpenDSS. The result of the power flow gives for each operation point the voltage and current in every nodes. This result can be further used to evaluate if a grid constraint has been violated.

A constraint on the voltage rise is given by the *Technical Rules for the Assessment of Network Disturbances* (D-A-CH-CZ, Germany – Austria – Switzerland – Czech Republic) that states the relative voltage rise should stay below 3% in low voltage grid. This voltage rise should computed with all the loads set to zero and all distributed generation systems producing at their nominal capacity.

Some others constraints are given by the EN50160 standard. This standard gives several compliance limits whose a few of them can be found in table 12.

Table 12: EN50160 standards for LV grids (extract from [6])

| | |
|------------------------------|--|
| Power frequency | ± 1% for 99.5% of week -6%/+4% for 100% of week mean value of fundamental measured over 10s |
| Voltage magnitude variations | ±10 % for 95% of week mean 10 minutes rms values |
| Rapid voltage changes | 5% normal, 10% infrequently $P_{lt} \leq 1$ for 95% of week |
| Supply voltage dips | Majority: duration <1s, depth <60% Locally limited dips caused by load switching on : 10-50% |

Added to this, the lines ampacity and transformer loading give supplementary constraints. In the context of the this report only the constraints on the voltage deviation, lines and transformer capacity will be evaluated.

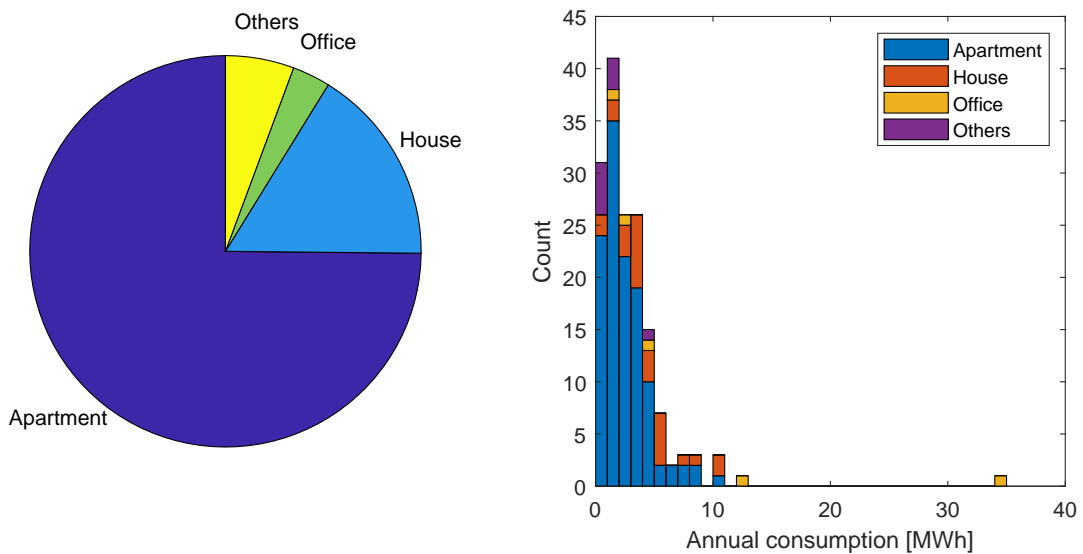
5. Results

5.1. Load allocation

This section presents the results of the load allocation model applied for the grid HOPITAL-TR3716 using the methodology introduced in section 4.2. This model required in particular for each node the measured annual consumption E_n^{REF} . These parameters have been derived from two data sources. The annual consumption of most nodes are the annual consumption measured by the electricity meters. However, the RCB (Registre Cantonal des Bâtiments) indicates that a few buildings have electric heating system and the corresponding meter cannot be identified. Consequently, the annual consumption measured by the meters in those buildings cannot be used.

The number of node per building is set to the number of flat given by the RCB. If an electric system is present or if the meter data are unavailable, the node annual consumption are statistically generated. For each building category (GKAT) the distribution of annual consumption of the corresponding valid meters have been fitted using a Weibull distribution.

The distribution of the node categories h_n for the HOPITAL-TR3716 grid is shown in the figure 16a. Most nodes, about 75% are labelled as apartments meaning that the allocated load profiles for those nodes come from load profiles measured in apartment in the context of the Flexi project.



(a) Nodes categories distribution in the HOPITAL-TR3716 grid

(b) Histogram of the annual consumption E_n^{REF} per node category

Figure 16: Inputs of the load allocation model

Unfortunately, since a full year load profile measured at the transformer for the HOPITAL-TR3716 grid is currently not available, only the first stage optimization of the load allocation has been conducted. The second stage optimization introduced in section 4.2 will be executed as soon as the data will be available.

A sample week of the sum of all profiles resulting of the allocation model is shown in figure 17a. The validity of the allocation model is not presented in the report. However the stochastic nature of the load profile is by construction preserved. This properties is fundamental for the grid stability assessment presented in section 5.4.

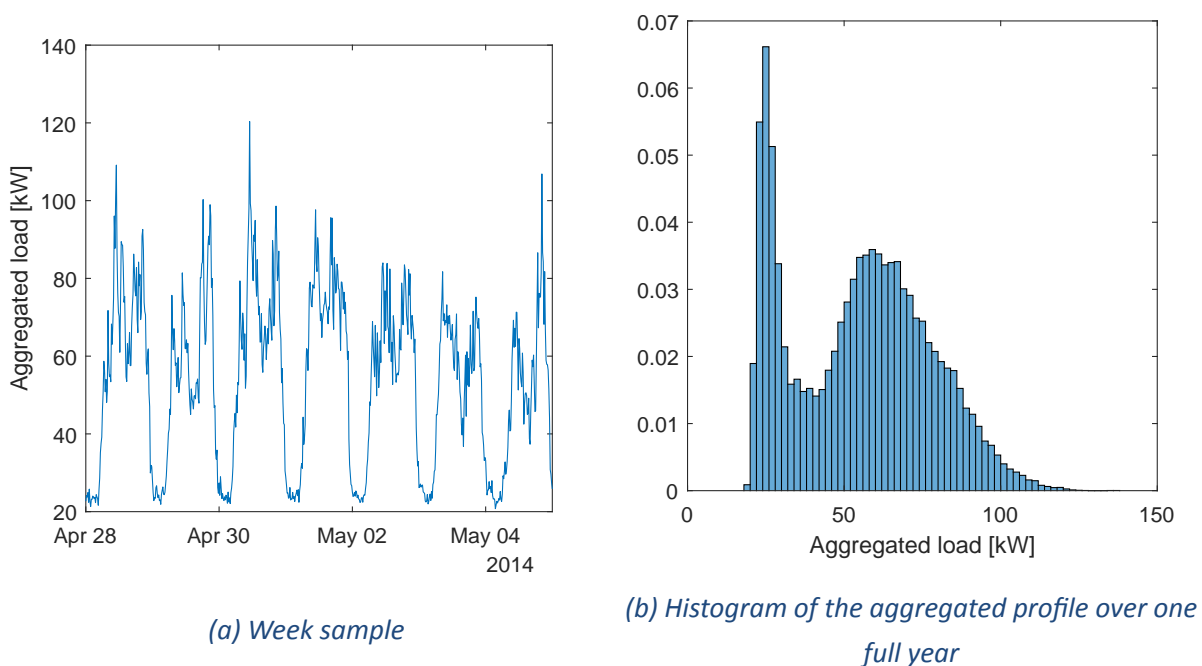


Figure 17: Output of the load allocation model - aggregated load profile

The histogram of the aggregation of all allocated load profiles over a full year is shown in figure 17b. The maximum grid load is about 120 kW, well below the transformer capacity of the considered grid rated at 400 kW. The first peak of the histogram corresponds with the mean standby consumption during the night.

5.2. Building's optimization results

Figure 18 shows the scenarios minimizing the CAPEX (Equation 19) for a range of possible investments values (Equation 19).

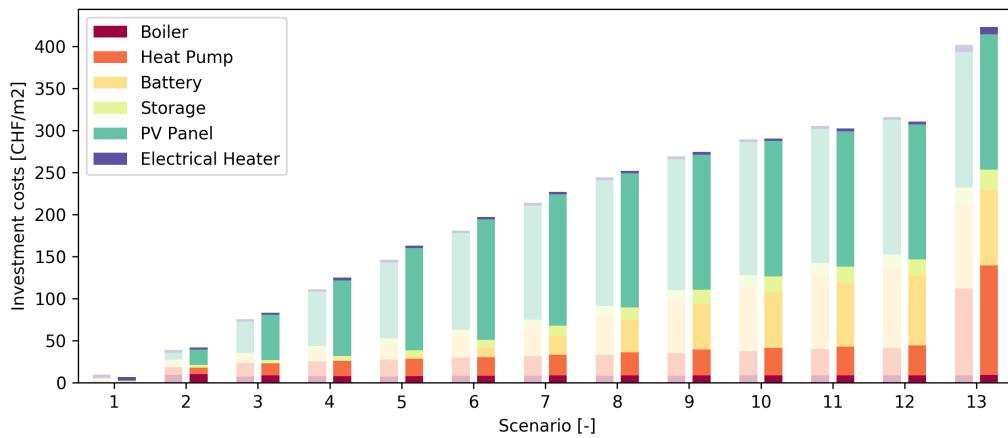


Figure 18: Optimal technological investment scenarios with (light, $\epsilon_{GM}=2$) and without (dark) grid peak constraint.

Figure 19 compares the annual energy flows (electricity and gas) of scenarios with and without grid peak constraint as a function of battery and PV penetration. One observes that the grid constraint ($\epsilon_{GM}=2$) favors the investment in batteries while postponing the investment in PV.

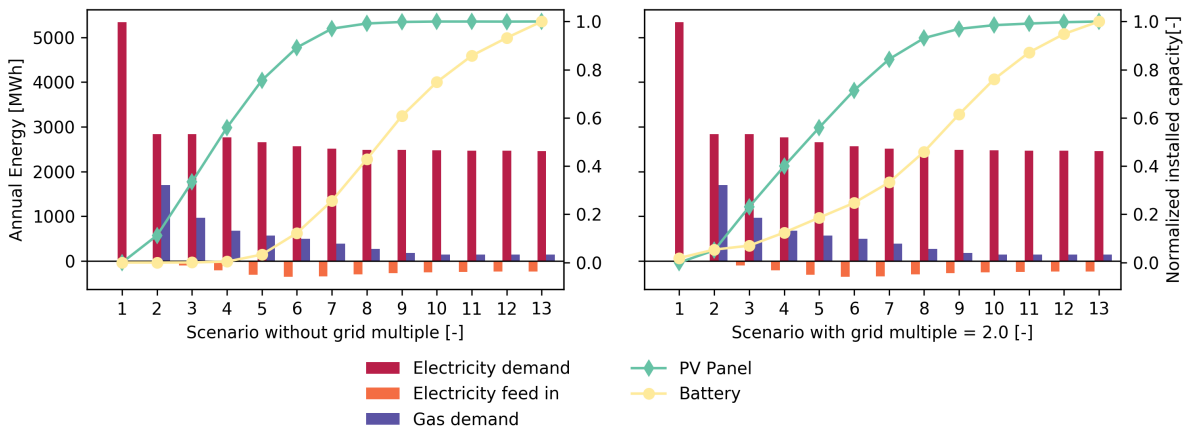


Figure 19: Annual energy flows as a function of battery and PV penetration without and with grid constraint ($\epsilon_{GM}=2$).

5.3. Load shifting potential

Behavioural flexibility

The results of the field experiment conducted in the flexi project are summarized in this section. The major outcome of this experiment is the difficulty of encouraging households to change the consumption habit. The reactions of the households are very different from one to another.

Some households reacted clearly in the direction promoted by the financial incentives while others performed counter-intuitively by increasing their consumption during high rate period and reducing their consumption during low rate period. These moderate results are put in perspective with the theoretical potential for flexibility.

Results of the field experiment

As summarized in section 4.4, a field experiment was conducted on a representative panel of Swiss households from the Jura region. Two alternatives pricing was experienced, the first was a reduction during 11 a.m to 3 p.m while the other was a dynamic tariff, i.e the low rate time window was changing every day. The reactions of both treatments are compared to a control group which received no information about the experiment.

As an illustration of the obtained reaction of the households, figure 20 depicts the median normalized daily profile of the first wave of the treatment 1 group. The curve of figure 20 must be interpreted as the median distribution of the energy across a day. A cross comparison between the blue and red curve (corresponding to the group T1 and control respectively) with the full and dashed line (before the experiment and after the experiment respectively), emphasize that no major reaction of the treatment group is observed with respect with the control group. No significant increase in the consumption is observed during the low rate period (the price curve is materialized on the right axis), while a slight reduction of the consumption during the evening is observed.

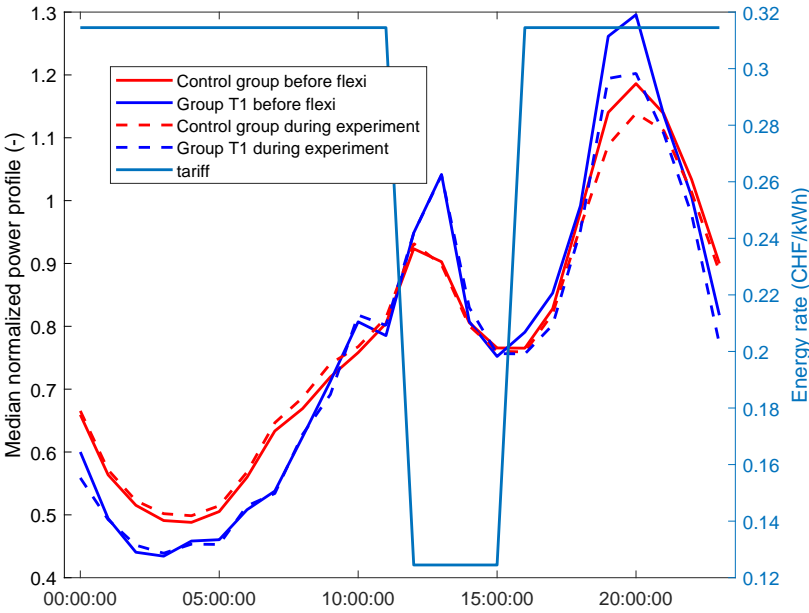


Figure 20: Normalized power profile group T1 wave 1

The evolution of the performance metrics (flexi score and daily energy consumption) are

a more representative indicators of the households reaction. In order to illustrate the underlying procedure, figure 21 draws a performance map for the first wave of the first treatment group. On the x-axis lays the mean daily energy consumption for each individual household and on the y-axis lays the average flexi score. A blue square represents the performance with respect to these metrics before the experiment starts and is linked to a red cross picturing the performance during the experiment. It is clear from this picture that some households were strongly involved in the experiment, as they both reduced their energy consumption and/or increase their flexi score. However, a few households reacted oppositely and increase the mean energy consumption and decrease their flexi score. The relative progression with respects to both metrics (flexi score and mean daily consumption) is reported on figures 22, 23 and 24 for each wave of the first treatment group (as a reminder, the first treatment group experienced fix low-rate times). As all the waves haven't started at the same date (see table 8, it's not possible to make a consistent comparison between them and the control group (which performance vary when changing the study windows).

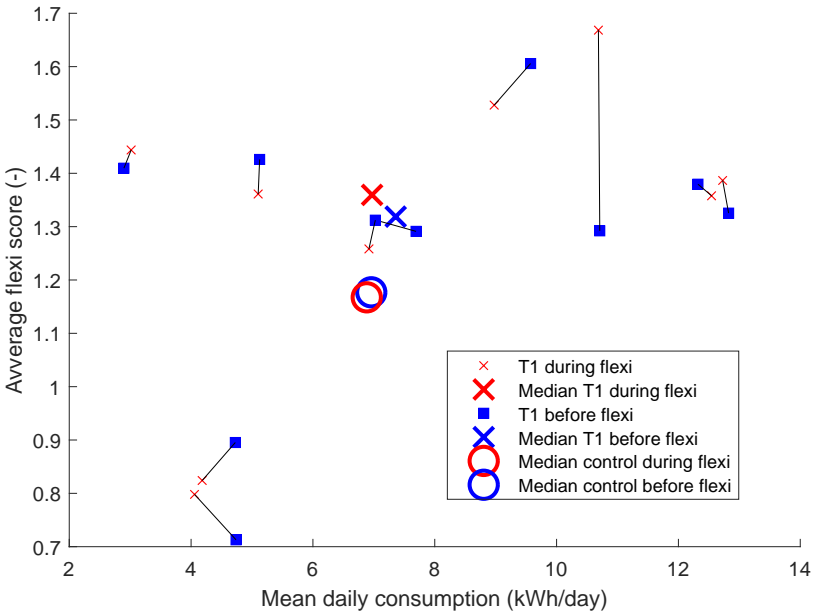


Figure 21: Performance of treatment group 1 wave 1

Each of these figures (figures 22, 23 and 24) is divided into four quadrants. The households (black cross) laying in the top left quadrant increased their flexi score and reduce their energy consumption. On the opposite, the households laying in the bottom right quadrant lowered the flexi score and increased their energy consumption. The numbers indicated in each quadrant represent the fraction of households located in each quadrant. In general, the fraction of households who increased their flexi score is higher for the treatment group than for the control group (50%, 50% 53%, for T1 group, wave 1, 2 and 3 respectively versus 45%,44%,46%

for the control group). However, this increase in the flexi score does not come with a reduction of the daily energy consumption but may also induce additional energy needs.

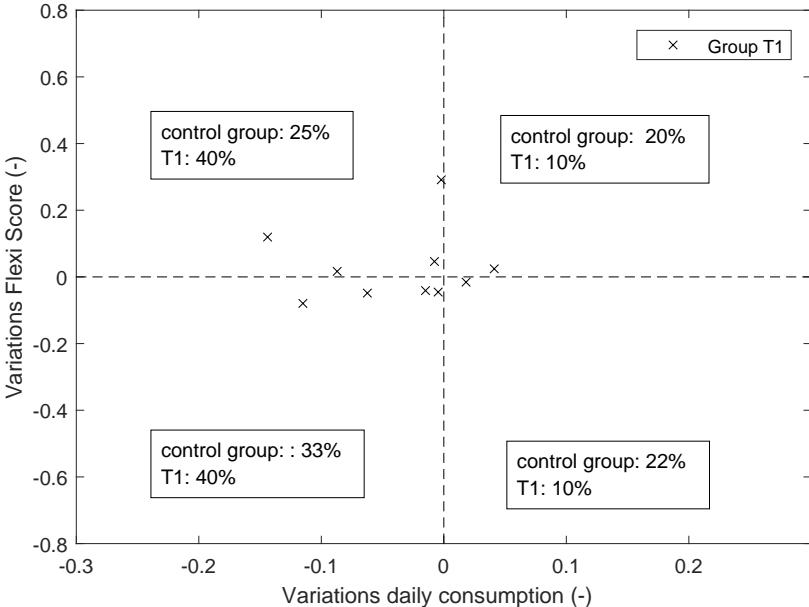


Figure 22: Performance variations of treatment group 1 wave 1

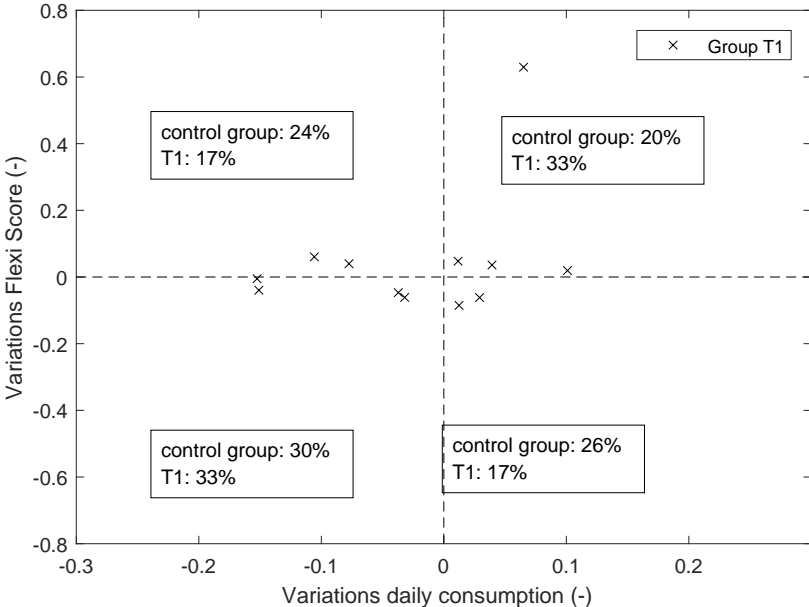


Figure 23: Performance variations of treatment group 1 wave 2

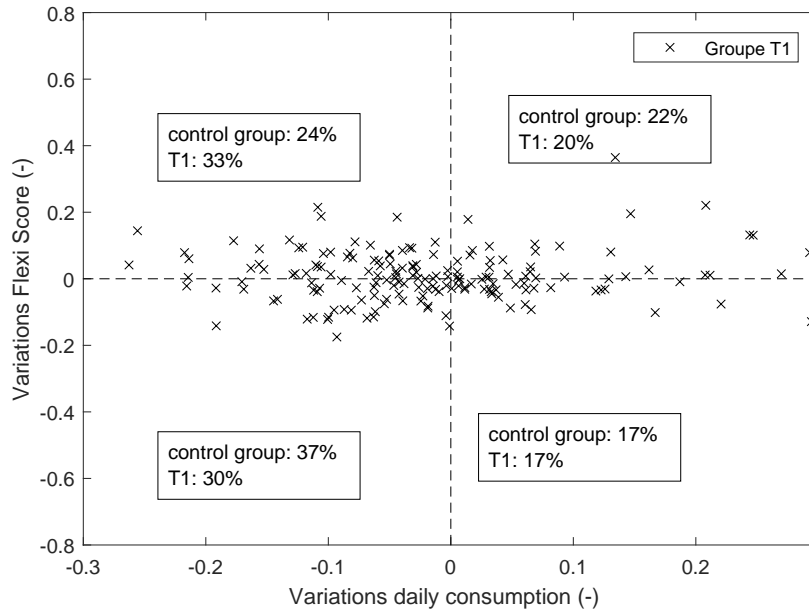


Figure 24: Performance variations of treatment group 1 wave 3

A similar analysis can be performed for the second treatment group (who experienced variable low-rate windows). Although the number of households is much smaller, a clear trend toward both a reduction of energy consumption and an increase in the flexi score can be observed.

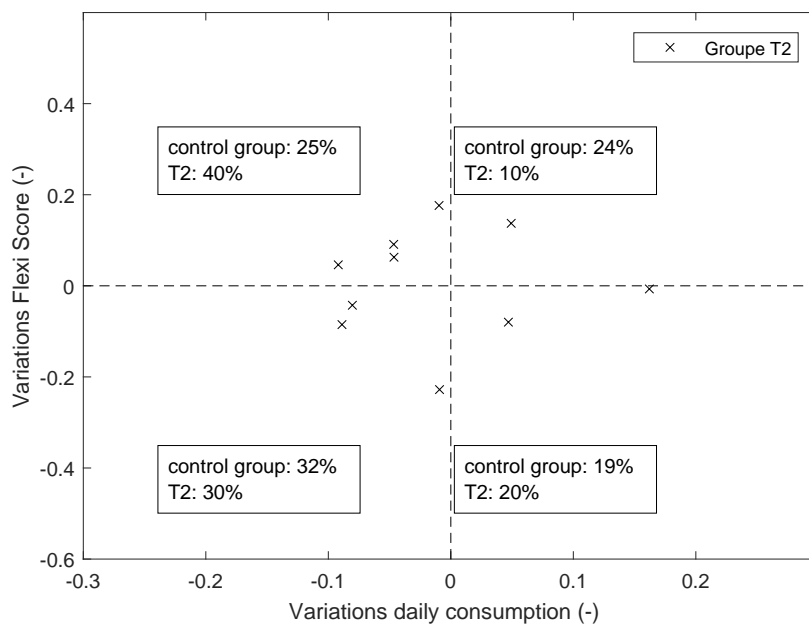


Figure 25: Performance variations of treatment group 2 wave 1

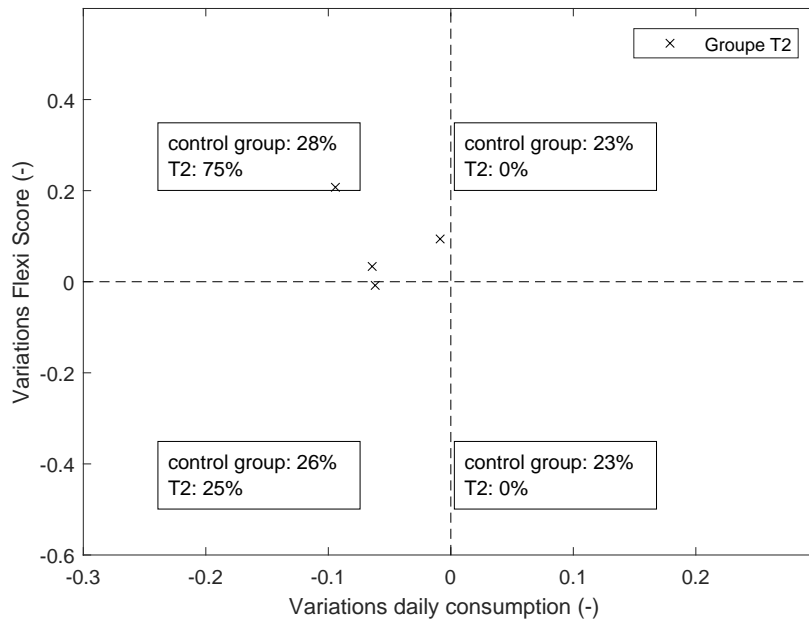


Figure 26: Performance variations of treatment group 2 wave 2

A general observation of these results showed a trend toward a positive reaction of the households to the provided incentives. However, as illustrated in the example of figure 20, these reactions do not distinguish themselves from the unpredictable and stochastic change in consumption habit (which measured by the control group). It is now interesting to show how these results are put in perspective with the theoretically achievable score.

Results of the theoretical flexibility

Following the methodology defined in section 4.4, the disaggregation of the profiles of the households provided some interesting answer to a few essential questions. A first is to check whether the load shifting potential is greater during the weekend than during weekday. Table 13 provides an answer by showing that the fraction of easy and hardly shiftable energy is slightly bigger during the weekend than during weekday although this difference is less than 2% of the total energy share. This hence justifies the fact that no analysis was carried out on the difference between weekend and weekday pattern.

Table 13: Share of energy according to their shiftable potential

| Share of energy... | Weekday | Weekend |
|--------------------|---------|---------|
| Easily shiftable | 6.45% | 6.87% |
| Hardly shiftable | 16.75% | 18.05% |
| Not shiftable | 76.80% | 75.08% |

The level of achievement defined as the ratio between the flexi score (as defined in equation

26) and the theoretical flexi score as defined in equation 27 is reported on figure 27 for the first treatment group and on figure 28 for the second treatment group. It as to be noted that this level can be, in some particular case, greater than 1 as the disaggregated energy may be smaller than the measured energy (as it is the case in the illustration of figure 11. As reported on table 14, all achievement levels are decreasing when going from the period before the experiment starts to the period after the start of the experiment, except for the second wave of the second treatment group. However, this decrease is lower for all treatment group. The households did somehow react to the financial incentives but for some external reason, their performance with respect to the flexi score didn't improve in absolute value but decrease at least in a moderate way with respect to the control group.

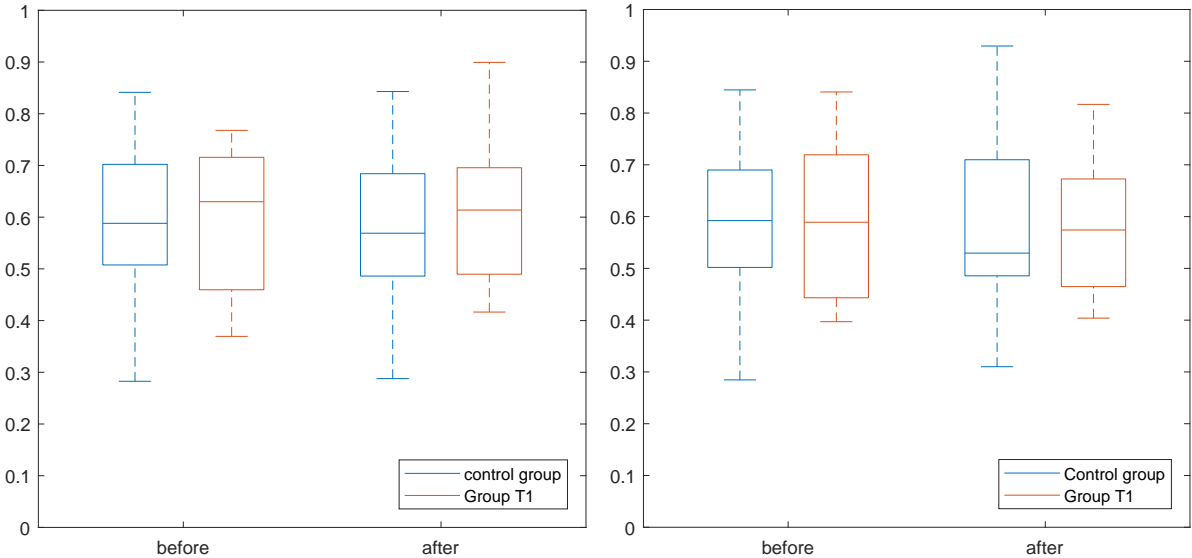


Figure 27: Level of achieved flexibility for treatment 1

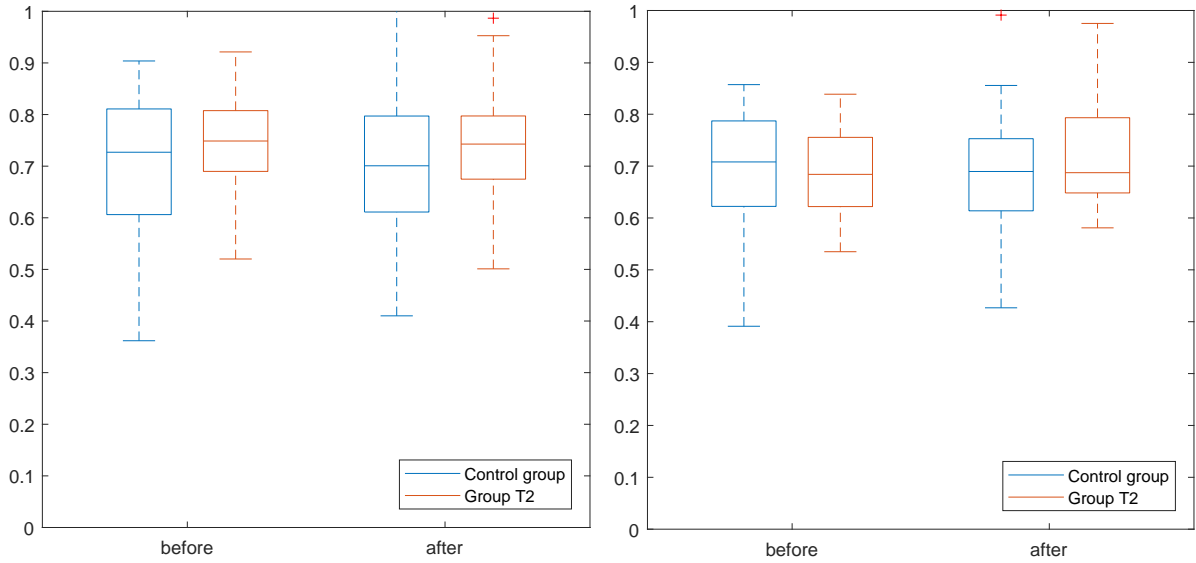


Figure 28: Level of achieved flexibility for treatment 2

Table 14: Median level of flexibility achievement for all groups and waves (%)

| | | Treatment 1 | | | Treatment 2 | | |
|--------|-----------------|-------------|-------|-------|-------------|-------|-------|
| | | before | after | delta | before | after | delta |
| wave 1 | Control group | 58.8 | 56.9 | -1.9 | 59.2 | 52.9 | -6.3 |
| | Treatment group | 63 | 61.4 | -1.6 | 58.9 | 57.4 | -1.5 |
| wave 2 | Control group | 72.7 | 70.1 | -2.6 | 70.8 | 69 | -1.8 |
| | Treatment group | 74.9 | 74.2 | -0.7 | 68.4 | 68.7 | 0.3 |

These results show how a practical field trial for demand-side management impacts the consumption of individual households. The results, however, show moderate results in term of improvement of the flexibility score of both treatment group with respect to the control group.

Theoretical behavioural flexibility equivalent storage

The aim of this section is to find what would be the equivalent storage of the theoretical behavioural flexibility. The flexibility of the allocated load profiles on the HOPITAL-TR3716 grid has been computed as described in section 4.4. Then this flexibility can be used to maximize the PV self-consumption, considering here all the grid as one self-consumption community. The daily shifted energy is, therefore, only a function of the PV generation profile of the day.

Considering the load at the transformer during a day, and the total PV generation in the network (for a given PV penetration), a flexi window (similar to the one defined in section 4.4)

is defined when the PV generation is greater than the load. In other words the flexi period is defined as the time when reverse power flow occurs. One has to note that multiple flexi periods in one day might occur. The quantity of shiftable energy, determined as described in section 4.4, is also known for each household of the network and will be shifted in the current flexi period in order to increase the self-consumption. This relies on the optimistic assumption that the shiftable energy can be moved anytime and distributed according to the reverse power flow profile (recalling that the conservation of energy still holds). This assumption allows finding an upper bound of the impact of the behavioural flexibility on the self-consumption. For each day, it is hence possible to evaluate the fraction of shifted energy relative to the average daily energy consumption of the network. The distribution of this fraction is plotted for four penetration level in figure 29.

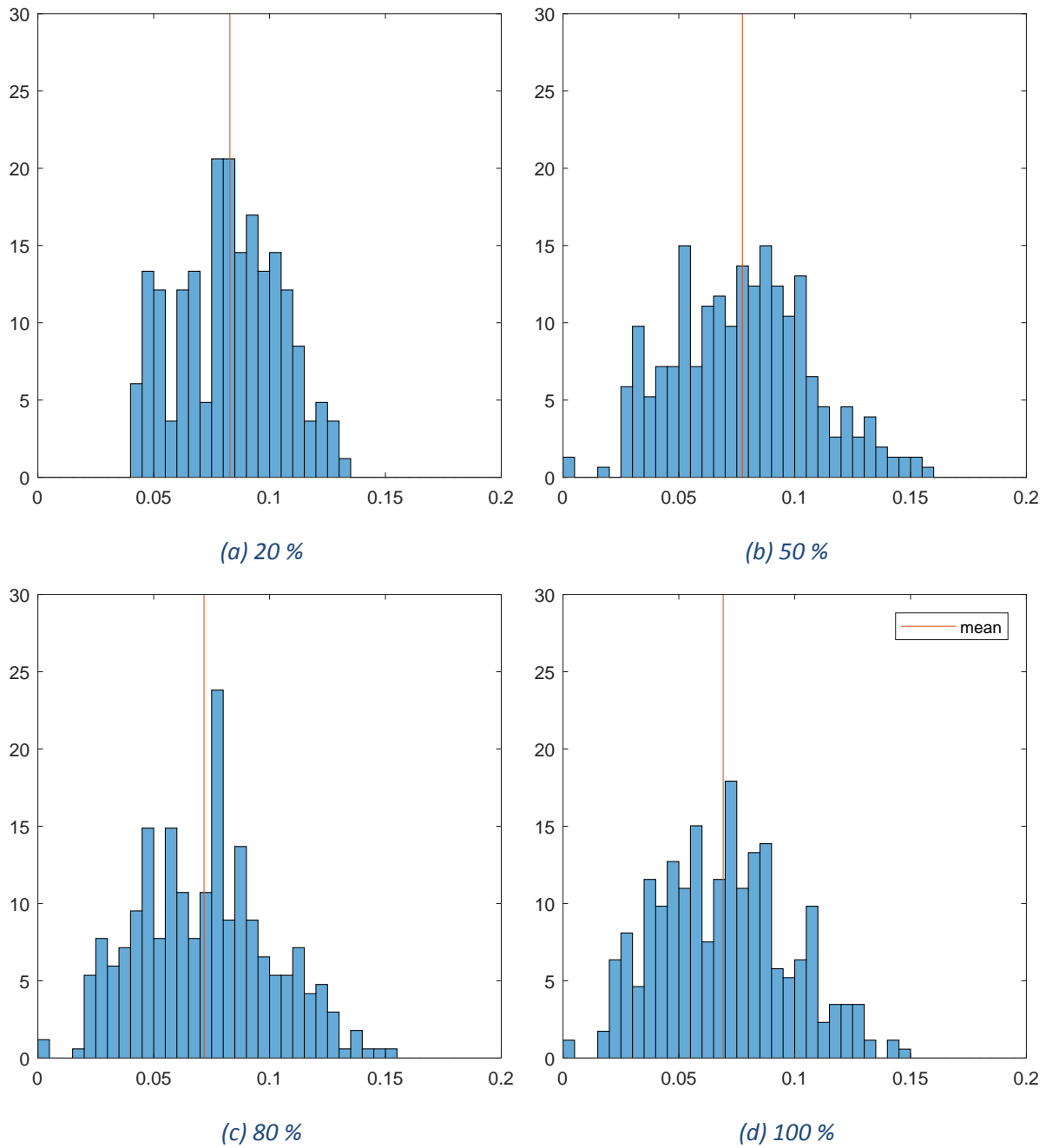


Figure 29: Ratio between the total shifted energy and the mean daily energy consumption of the network for the different penetration levels. The y axis is the number of days.

The results showed in figure 29 doesn't indicate a very large variation with respect to the penetration level. The maximum of the ratio laying around 16%. For a mean daily energy consumption of about 2 MWh this is equivalent to a storage capacity of 315 kWh.

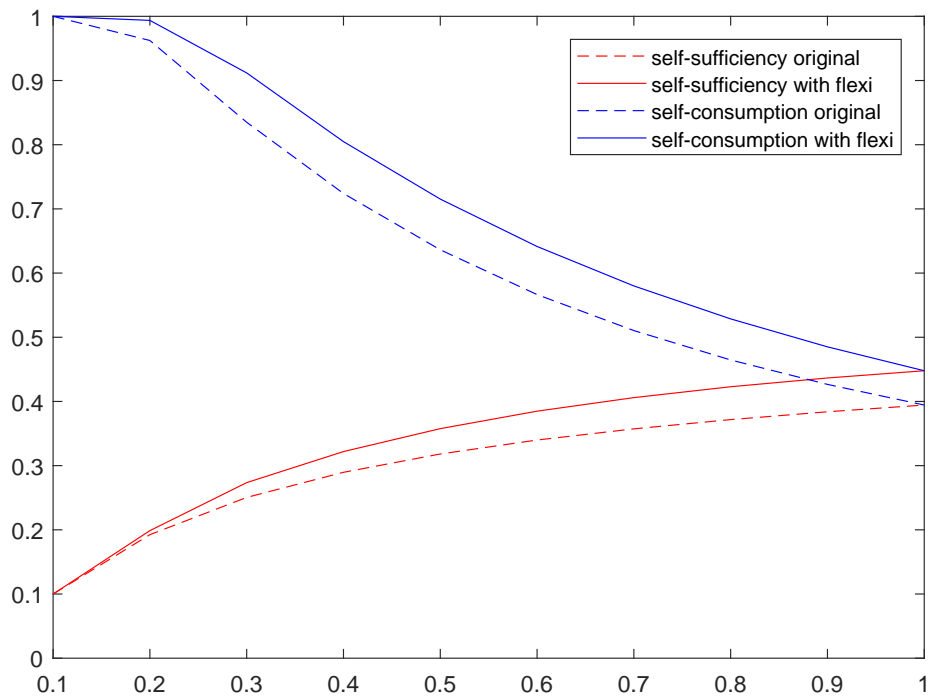


Figure 30: Self consumption and self sufficiency as a fonction of the PV penetration level for the original case and the optimal use of the theoretical flexibility.

The self-consumption level and self-sufficiency level have been reported in figure 30 for a PV penetration level between 10 and 100 % emphasizing the added value of the flexibility. Indeed the self-consumption increase up to 8 % at a PV penetration of 40% and both self consumption and self sufficiency increase by 5% at 100 % of PV penetration (39 % originally 44% with the theoretical flexibility).

Operational flexibility

Figure 31 shows the flexibility potential of the Hopital-TR3716 district for an installed capacity of 100% PV and 40% of battery (see scenario 8, Figure 18). The high penetration of PV generates high charging peaks at mid-day and high discharging peaks in the morning.

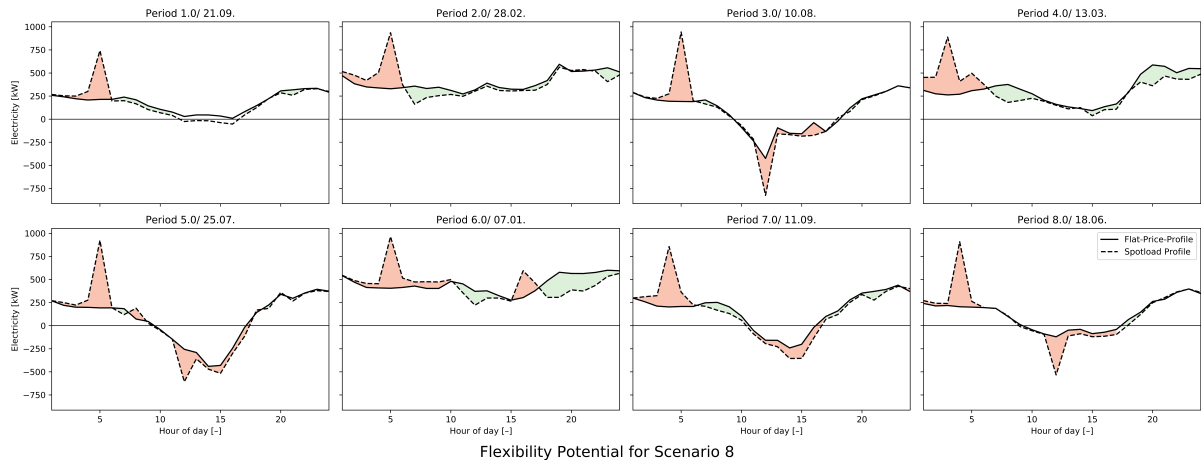


Figure 31: Operational flexibility for a PV Penetration of 100% (without grid constraint) - optimal operation with flat electricity price (continuous line) and spot-load price (dashed line).

Technical flexibility

The technical flexibility is assessed by comparing the virtual batteries characteristics between different investment scenarios. Figure 32 and 33 presents the technical flexibility of the Hopital-TR3716 district grid with and without the grid peak constraint defined by Equation 20). The flexibility potential increases as a function of the PV and batteries installed capacity. The penetration of PV correspond to a positive annual capacity while batteries to negative capacity.

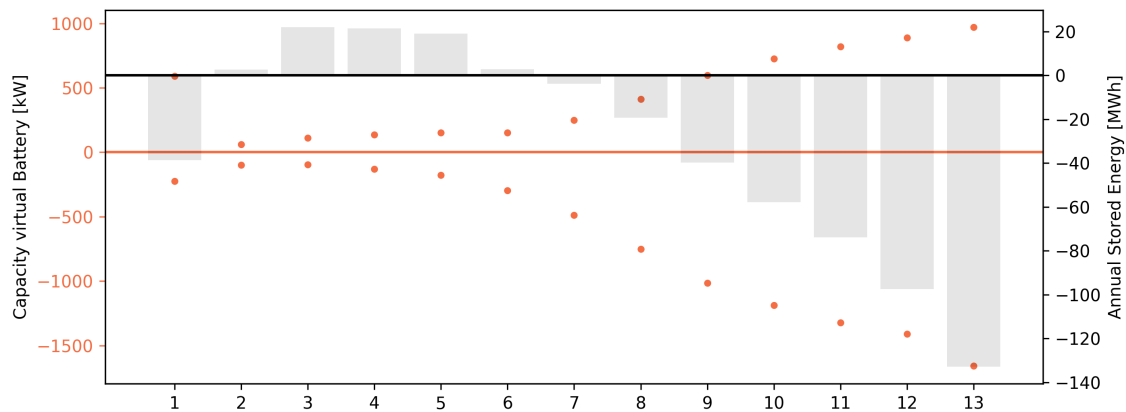


Figure 32: Capacity (orange) and annual stored energy (grey) of the district grid virtual battery for each energy transition scenario without grid constraint.

The introduction of grid peak constraint (ϵ_{GM}) favors the installation of batteries, thus increasing the flexibility of the low investment scenarios while restraining the flexibility potential of the grid in the long term.

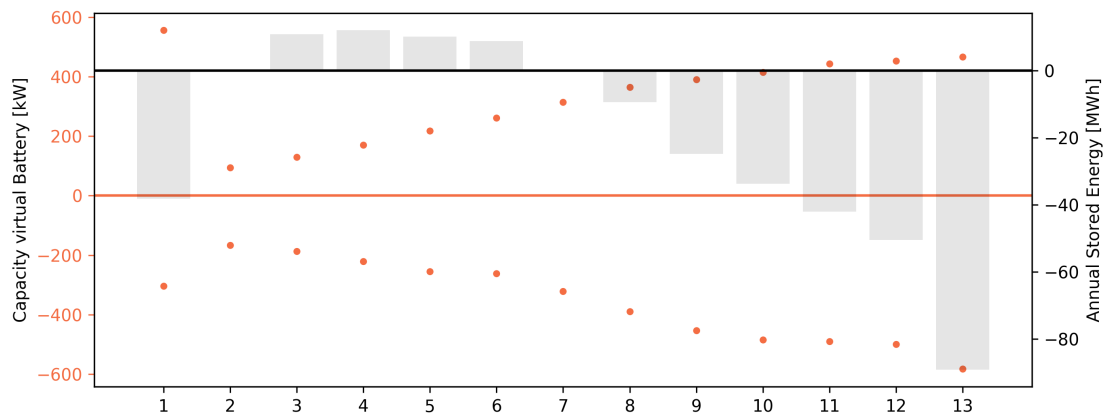


Figure 33: Capacity (orange) and annual stored energy (grey) of the district grid virtual battery for each energy transition scenario with grid constraint ($\epsilon_{GM}=2$).

5.4. Grid operation bottlenecks

This section presents the evaluation of the grid bottlenecks considering the grid constraints introduced in section 4.5. The considered system in the following analysis is represented in figure 34 that shows both LV and MV grids and the buildings connected to the selected HOPITAL-TR3716 low voltage grid. The first part is focusing on the grid bottlenecks in case of high penetration of PV. In the second part the penetration and feasibility of a selected scenario resulting of building MILP optimization is presented.

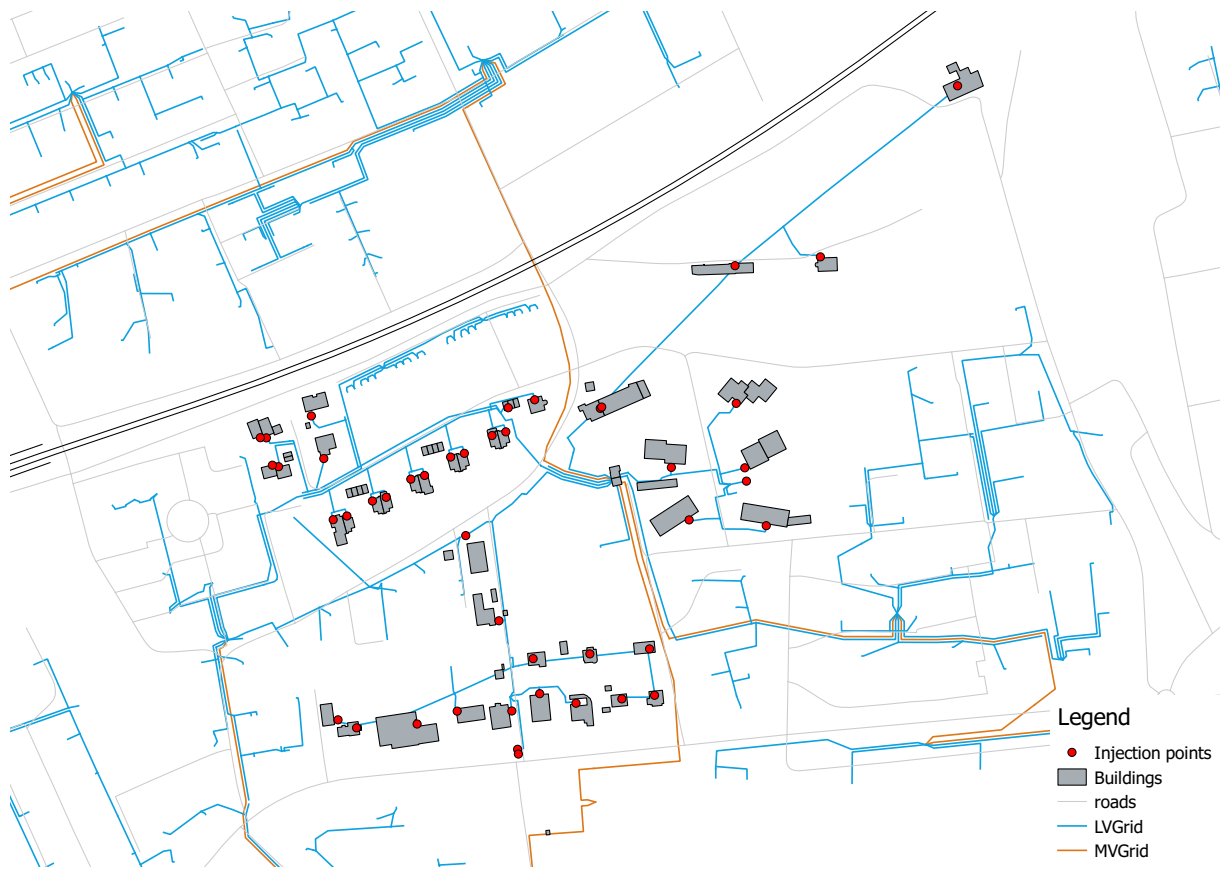


Figure 34: GIS diagram of the low voltage (blue) and medium voltage (orange) grids as well as the buildings connected to the low voltage grid HOPITAL-TR3716 and their injection points.

PV hosting capacity

A first approach to identify the grid bottlenecks is to compute what would be the PV hosting capacity of the selected grid considering individually each grid constraint. In this first approach, the electricity demand is neglected, only the generation is considered in order to apply the DACHCZ limit for the voltage deviation.

The installation order of the PV systems has a large influence on the PV hosting capacity of the grid. If a large PV system is installed at the end of a weak line, some grid constraint can already be violated. Although it is feasible to find a configuration that maximizes the PV hosting capacity, such configuration is unlikely in a real residential grid since the choice to invest in a PV system belongs to the building owners and not to a centralized organization or to the distribution system operator (DSO). For this reason, we assume in this section that PV systems with the highest energy yield are installed first. In this way, best-oriented roofs are firstly selected until one of the grid constraints is reached. When this happens, the last roof system is removed in order to avoid being limited by a specific configuration and the iteration continues until all the roofs have been considered. This procedure is repeated for three grid constraints, voltage

deviation (DACHCZ), line loading and transformer loading.

The results reported in table 15 show that considering only the transformer loading allows a much higher PV capacity compared to the two others constraints. Indeed with a PV capacity of 415 kW, the transformer capacity would be reached, however the maximum voltage deviation over all the nodes is already two times higher the accepted deviation. Similarly, the maximum line loading would reach 180% meaning that the current is 1.8 times the accepted one.

Table 15: PV hosting capacity in the grid HOPITAL-TR3716 for each grid constraint

| PV on the roof of buildings | PV Penetration (capacity) | Voltage deviation | Line loading | Transformer loading |
|-----------------------------|---------------------------|-------------------|--------------|---------------------|
| voltage | 248 kW | 100% | 109% | 61% |
| line | 228 kW | 129% | 100% | 55% |
| transformer | 415 kW | 201% | 180% | 100% |

In the limit of this approximation, both voltage and line constraints are expected to be reached before the transformer capacity.

Grid stability assessment under the deployment of a selected scenario

If all buildings in the selected grid would follow the same scenario, no scenario would satisfy the grid constraints. Figure 35 shows the active power at the transformer point whose nominal capacity is 400 kW. A negative power represents a reverse power flow from the LV to MV grid. For each scenario, the power exceeds the limit [-400 kW,400 kW] during at least one period.

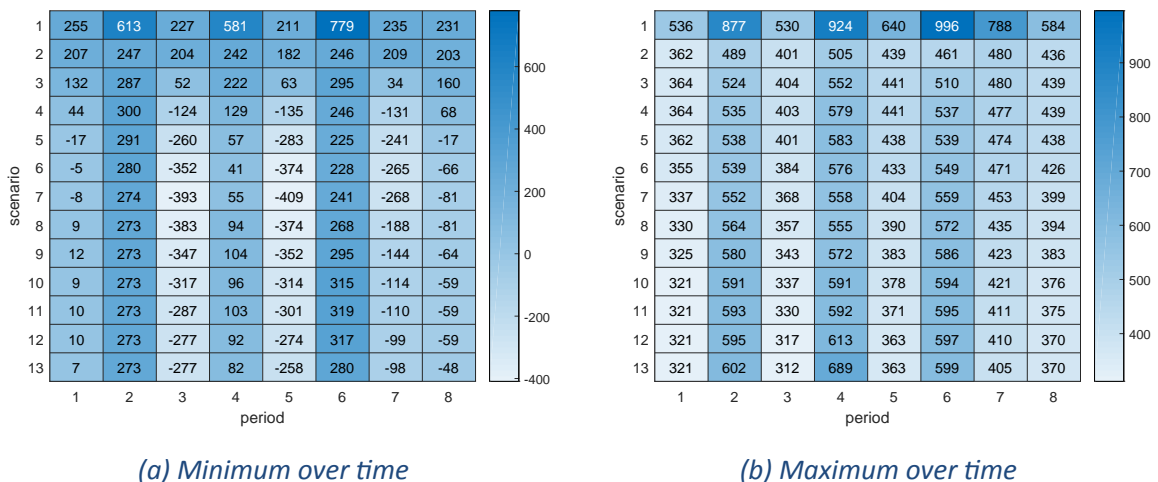


Figure 35: Active power (kW) at the transformer assuming that every building are following the same scenario and period. A negative value represents a reverse power flow from the LV to MV grid.

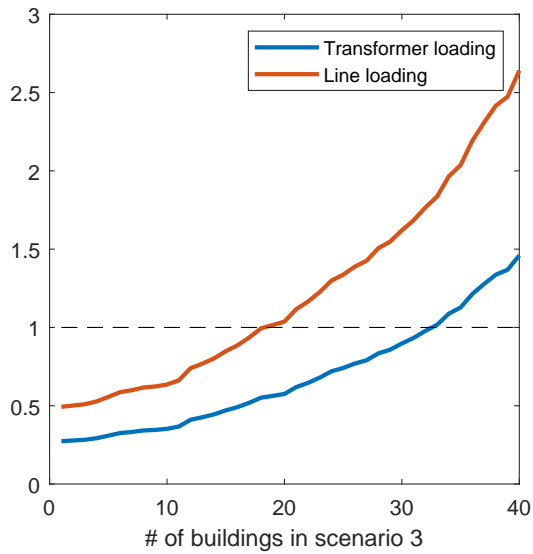
Since the scenario where all loads are given by the load allocation model satisfies the grid constraints, we can evaluate from the grid stability point of view what would be the highest penetration of a selected scenario. For each building either the default load profile from the allocation model is chosen or the load profile resulting from the MILP optimization for a selected scenario. Then, considering the grid constraints the maximum share of buildings under the selected scenario can be determined.

Obviously, the maximum share depends on the buildings selection. This selection could be done randomly but the approach here is to choose a criterion in order to decrease the computing time to solve the power flows. Then the buildings can be ordered according to this criterion similarly the energy yield criteria for roofs in the PV hosting capacity evaluation. The idea is to order them on their marginal impact on the grid. For this the line loading defined in equation 33 was computed where all grid exchanges are set to zero excepted for the considered building for which the grid exchange is equal to the highest value over the periods and times of the selected scenario ($L_b^{wc} = \max_{p,t} L_{b,p,t}$). Then the buildings are ordered accordingly to this criteria, meaning that buildings with the lowest marginal impact on the line loading are selected in priority.

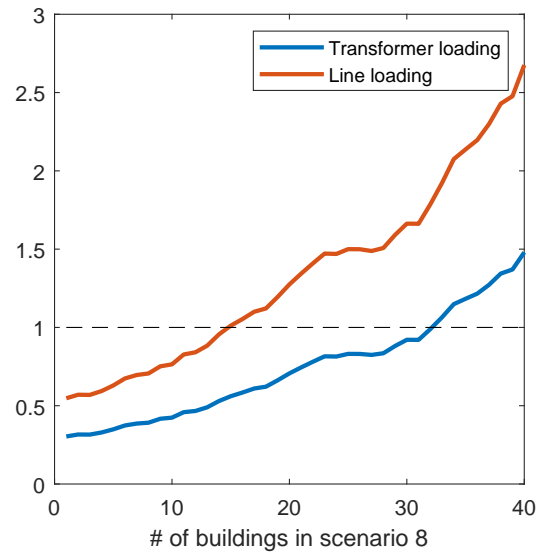
$$\text{line loading} = \max_{l,p,t} \frac{I_{l,p,t}}{I_l^{\text{NOM}}} \quad (33)$$

Where $I_{l,p,t}$ is the current in the line l for the period p at time t and I_l^{NOM} is the ampacity of the line l .

Figure 36 shows for scenario 3 and 8, the evolution of the transformer and line loading in function of the number of buildings following the selected scenario. Loading higher than 1 means for the transformer that the absolute power is above 400 kW and for the line that at least one line is overloaded. For both scenarios, the line constraint is reached before the transformer constraint. Due to the line constraint, only 19 and 15 buildings over the 40 considered could follow scenario 3 and 8 respectively. A higher share would require to reinforce at least one line.



(a) Scenario 3, GM = 2



(b) Scenario 8, GM = 0

Figure 36: Transformer and line loading in function of the share of buildings following a selected scenario

The voltage deviation constraint has not been considered here due to the temporal resolution of the MILP results. The EN50160 require to evaluate the voltage over a week at a resolution of 10min. However, the MILP result gives the grid exchange only for a period of one day at a resolution of one hour.

6. Conclusion

This work set the basis for the elaboration of energy transition guidelines, providing materials for other project partners to elaborate investment schedule and business models for the future development of the Swiss electrical infrastructure.

From a practical point of view, the combination of geographical data with modelling results has found use as a valuable decision making tool to target region and users for the development of the REel Demonstrator Community.

In order to overcome the poor availability of electricity demand profile in distribution grid, either due to the missing smartmeter infrastructure or for confidentiality issues, an allocation algorithm has been developed to evaluate with sufficient precision the integration of energy technologies in buildings. Since real load profiles are used, the stochastic nature of the demand is preserved enabling the possibility to generate optimal energy transition scenarios at the grid scale, showing trends between self-consumption, self-sufficiency, investment and operation cost.

The practical behavioural flexibility of the demand has been quantified in the context of the FLEXI project, showing a visible reaction from households to the incentive. The theoretical potential of the electricity demand behavioural flexibility has been quantified by disaggregating the demand into several appliance categories. Considering ideal harvesting of this flexibility, an average of the 7% of the daily demand consumption at the grid scale could be shifted to increase PV self-consumption.

Grid constraint has been considered at two levels: (i) in the control of the electric power system through a grid multiple (GM) factor for peak shaving and (ii) in the infrastructure using a power flow algorithm to address the grid operation bottleneck. It has been shown that increasing the hosting capacity of PV in the grid would activate both voltage and line constraints before reaching the transformer capacity.

At a theoretical level, a new approach has been proposed to quantify the various sources of flexibility in the grid. The method relies on the definition of an equivalent virtual battery to measure and compare the present and future load shifting potential, taking into account the evolution of the power grid.

Foreseen improvements of the method include:

- the validation on IEEE networks of the load allocation model;
- the introduction of a stochastic model for the hot water production and heating demand;
- the integration of electro-mobility;

- the consideration of the inter buildings shadowing effect and PV potential in facades;
- the development of a method for the identification of extreme operating conditions;
- the identification of the cheapest grid reinforcement solutions;
- the use of thinner temporal resolution to evaluate the voltage constraint accordingly to the EN50160 standard.

References

- [1] Christoph Bucher. *Analysis and Simulation of Distribution Grids with Photovoltaics*. PhD thesis, ETH-Zürich, Zürich, 2014.
- [2] Assemblée fédérale de la Confédération suisse. Loi sur l'énergie (lene) 730.0 du 30 septembre 2016, Etat le 1er janvier 2018.
- [3] International Energy Agency (IEA). *Linking Heat and Electricity Systems - Co-generation and District Heating and Cooling Solutions for a Clean Energy Future*. Technical report, 2014.
- [4] International Renewable Energy Agency (IRENA). *Power System Flexibility For The Energy Transition*. Technical report, 2018.
- [5] Raymond Kohli, Anouk Bläuer Herrmann, Silvia Perrenoud, and Jacques Babel. *Les scénarios de l'évolution de la population de la Suisse 2015 – 2045*. Technical report, Office fédéral de la statistique (OFS), Neuchâtel, 2015.
- [6] Henryk Markiewicz and Klajn, Antoni. *Standard EN 50160 Voltage Characteristics in Public Distribution Systems*. Technical report, Wroclaw University of Technology, 2004.
- [7] L. Middelhaue, F. Baldi, L. Bloch, and P. Stadler. *Influence of photovoltaic panel orientation in modern energy system*. *ECOS Conference Proceeding*, 2019.
- [8] Luise Middelhaue, Lionel Bloch, Luc Girardin, Paul Stadler, Jordan Holweger, and Hervé Tommasi. *Design of Sizes for Buildings Energy Systems as a Function of the Grid Evolution*. Technical report, EPFL Valais/Neuchâtel, 2018.
- [9] Mathias Niffeler, Thomas Schluck, and Curdin Derungs. *Analysis of initial case and identification of potential use for renewables and waste heat at the building and district area*. Technical report, Hochschule Luzern (HSLU), Lucerne, 2018.
- [10] Office fédéral de l'énergie (OFEN). *Feuille d'information sur l'énergie no 5. La Stratégie énergétique 2050*. Suisseenergie edition, 2015.
- [11] Office fédéral de l'énergie (OFEN). *Statistique globale suisse de l'énergie 2017*. Technical report, 2018.
- [12] Stadler Paul. *Model-based sizing of building energy systems with renewable sources*. PhD thesis, EPFL, 2019.
- [13] Jakob Moritz Fabian Rager. *Urban Energy System Design from the Heat Perspective using mathematical Programming including thermal Storage*. PhD thesis, École Polytechnique Fédérale de Lausanne, 2015.

- [14] P. Stadler, L. Girardin, and F. Marechal. "The Swiss Potential of Model Predictive Control for Building Energy Systems". 2017.
- [15] Paul Stadler, Araz Ashouri, and François Maréchal. "Model-based optimization of distributed and renewable energy systems in buildings." *Energy and Buildings*, 120:11. 103–113, 2016.
- [16] Paul Stadler, Luc Girardin, Araz Ashouri, and François Maréchal. "Contribution of Model Predictive Control in the Integration of Renewable Energy Sources within the Built Environment." *Frontiers in Energy Research*, 6, 2018.
- [17] David Stickelberger. *Solarpotenzial Schweiz - Solarwärme und PV auf Dächern und Fassaden*. Zürich, swissolar edition, 2017.